SQUID sensor design

By:

Martina Tsvetanova

GRADUATION REPORT

Submitted to
Hanze University of Applied Science Groningen

in partial fulfillment of the requirements
for the degree of

Full time Honours Bachelor Advanced Sensor Applications

Sunday 21st June, 2015

Abstract

The current report concerns the research on a SQUID sensor design for the detection of magnetic monopoles in topological insulators. The focus of the project was to evaluate the potential sensor parameters and investigate the possibilities for its fabrication, considering the available resources at the University of Twente, Enschede, the Netherlands. Possible magnetic monopole detection methods were reviewed and compared, showing that a SQUID is one of the best approaches for the task.

Theoretical analysis provided the ranges for a potential sensor parameters and those were implemented in the further work. Considering the available materials and facilities, the decision was taken to fabricate and test Nb/Al/AlO_x/Al/Nb Josephson junctions based SQUIDs with variable dimensionality. In the process of fabrication, the limitations and further considerations for a SQUID integration in a topological insulator device were identified and summarized.

Measurements yielded successful Josephson junctions but there was not enough experimental proof for the identification of a functional and suitable SQUID for the purpose of magnetic monopole detection. Therefore, the possibilities for improvements on the process of fabrication were investigated. Based on the observations, major alterations need to be done only with respect to the design execution strategy and procedural adjustment.

DECLARATION

I hereby certify that this report constitutes my own product, that where the language of others is set forth, quotation marks so indicate, and that appropriate credit is given where I have used the language, ideas, expressions or writings of another.

I declare that the report describes original work that has not previously been presented for the award of any other degree of any institution.

Martina Tsvetanova

ACKNOWLEDGEMENTS

I take this opportunity to express my gratitude to my supervisors Prof. Dr. Ir. Alexander Brinkman (chair QTM group, University of Twente) and Joris Voerman (MSc, ICE group, University of Twente), who provided me with the opportunity to work on this project and shared their expertise which greatly assisted my work. Additionally, I would like to acknowledge the technical support of Dick Veldhuis (Ing, ICE group, University of Twente) and Dr. Martin Stehno (Post Doc, ICE group, University of Twente), whose advices helped in resolving many of the issues I encountered.

Contents

List of Abbreviations

- **SQUID**
  Superconducting Quantum Interference Device
- **ICE**
  Interfaces and Correlated Electrons
- **TI**
  Topological Insulator
- **MFM**
  Magnetic Force Microscope
- **RCSJ**
  Resistively and Capacitively Shunted Junction
- **RIE**
  Reactive Ion Etching
- **PCB**
  Printed Circuit Board
- **AFM**
  Atomic Force Microscope
- **SEM**
  Scanning Electron Microscopy

List of Definitions

In this section the reader can find definition of particular terms, appearing in the report.

1. SQUID

   Superconducting loop, interrupted by one or several Josephson junctions (introduced later). SQUIDs are devices, very sensitive to magnetic fields and this predefines their application as magnetic sensors. [1, 2]

2. Topological insulators

   Material which insulates on the inside but due to strong spin-momentum coupling has surface states allowing electron transport. This is a state of quantum matter behaving like an insulator in its bulk but as a metal on its surface.[3]

3. Magnetic monopole

   Magnetic monopole is an elementary particle which represents a single magnetic pole (or magnetic charge).[4]

4. Majorana fermion

   A particle with half integer spins allowed (as the other fermions) that is its own antiparticle. Majorana fermions are neutral in charge and one cannot distinguish a particle from its antiparticle. The existence of these fermions is predicted by the Italian physicist Ettore Majorana from where their name emerges.[5]

5. MFM

   Magnetic force microscopy (MFM) is a special case of the atomic force microscope (AFM). The microscopy of this kind is a surface technique. A magnetic probe, brought close to a sample interacts with the magnetic fields near the surface. The strength of the local interaction determines the vertical motion of the tip. Recording the motion is equivalent to recording the force of interaction.[6]

6. Dyon

   In topological insulators, the composition, consisting of an electron and its image monopole is a single particle, as the image monopole would not be present separate from the charge which induced it, or it is not an elementary excitation of the system. The combination of charge and monopole is a dynamic object, called a dyon.[7, 8]

7. Weak links

   A weak link is a connection between two bulk superconductors in which the superconductor‘s dimensionality is altered or complete different kind of material(s) is(are) deposited (normal metal, insulator, or combinations).

8. Josephson junction

   The Josephson junction is system of two weakly coupled superconducting electrodes. The weak links between the electrodes could be constructed of different materials and with different intentions, regarding their application, frequently to tune the supercurrent.[2, 9]

   Examples are:[2, 9]

   - SNS: Superconducting– Normal conducting– Superconducting layer. Oxide or other insulator is used.
   - SIS: Superconducting-Insulating-Superconducting layer. Layer of normal metal evaporated between two superconducting films.
   - Point contact junction: Superconducting wire ground to a point and allowed to get oxidized. Then the point is pressed against a bulk superconductor.

- Thin film micro bridge: The weak link between the two superconducting electrodes is a film, formed by particular processing of the superconducting material.

9. Cooper pairs

   The superconducting state of a metal is the energetically favoured state in which two electrons with opposite spins and momenta form a pair, known as a cooper pair. Such pairs (different from separate electrons) are allowed to have the same energy state.[10]

10. Quantum tunneling

    Similar to optics when we always have reflected and refracted beams of light, quantum mechanically there is finite probability to have a particle‘s wave function transmitted through (or reflected by) a barrier. This effect is not allowed in classical physics therefore the effect is called quantum tunneling.[11]

11. Bath cryostat

    Refers to system in which sample measurements are performed at very low temperatures (up to several Kelvin). Bath cryostates use cryogenic liquid (such as Helium or Nitrogen) in order to keep the system cold.

12. Lithography

    A process for patterning various layers, such as conductors, semiconductors, or dielectrics on a surface, including the application of photo-sensitive material (photoresist) on top of a sample and illuminating the sample under a mask of the desired pattern.[12]

13. Sputtering

    Sputtering is a method to deposit thin films of a material onto substrate. Plasma is created and its ions accelerated (by voltage difference) towards a target (source of material to deposit on a substrate). When the energy rich ions hit the target, atom clusters, single atoms or molecules are released. These then travel towards the substrate where a film is grown.[13]

14. Reactive ion etching

    Reactive ion etching is very similar to sputtering, but in this process material is removed from the substrate. Additionally, except the physical part of the process, the gases introduced in the etching also react chemically with the sample. This is how it is possible to selectively etch materials.[14]

15. Vortex (Abrikosov vortex)

    Type I superconductors obey the Meissner effect and expel magnetic field completely. Magnetic field can penetrate only up to some penetration depth characteristic for the material. In type II superconductors magnetic field can penetrate the material in the form of a vortex of minimal magnetic flux quantity. Vortices have normal metal core and are surrounded by screening currents.[15]

List of Tables

List of Figures

I. Rationale

The current graduation report concerns the design of a superconducting quantum interference device (SQUID) sensor for application in a magnetic monopoles detection set-up for topological insulator (TI) materials. The research took place at the ICE (Interfaces and Correlated Electron Systems) group at the University of Twente (Enschede, the Netherlands). Currently the topic of topological insulators is widely researched in the ICE science group and worldwide, with papers published almost daily.[1, 2] The reasons are connected to the fact that topological insulators are newly discovered and promising materials, reviewing possibilities to explain more phenomena in nature.[3] Understanding of these types of materials could lead to new generation of magneto-electric devices, and in combination with superconductors, to a new innovative view upon quantum computing.[4] Another importance of topological insulators is their potential contribution to theoretical physics, as hypothesized and researched effects in those types of materials predict the existence of many exotic particles, such as the magnetic monopole [5] or the "Majorana" fermion [6].

The detection of the magnetic monopole is the topic of interest for the research described in this graduation report. If proved to exist, the magnetic monopole would have enormous impact on the unison of physical theories [7] and that is why currently many scientific groups around the world claim its discovery or try to experimentally induce/measure it with various set-ups and in different materials.[8, 9, 10] This is the main prerequisite for the desire of the ICE group for the development of a SQUID sensor for monopoles detection. Two types of set-ups for the detection of magnetic monopoles have been already hypothesized.[5, 11, 12] In one of the experimental models a magnetic force microscope (MFM) is proposed, while the other possibility identified is a SQUID. The choice of SQUIDs as goal of the research is explained further in the next chapter, but some points can be as well identified here. The goal of the ICE group is to implement the monopole detection mechanism in rather mobile set-up which is easy to operate with minimal complexity of the readings.[13] Additionally, relevant experience and understanding of SQUIDs has been achieved by the former and current members of the group, as shown by the PhD theses produced in the collective of the topic.[14, 15] Moreover, the time allocated for the full monopole research is well beyond the period of the current graduation project, thus identifying the SQUID as non-satisfactory solution would still be useful result for the future.

The problems of the current research were the analysis of the theory and situation and the overview of the possible ways of designing a SQUID sensor for the purpose of the monopole detection. A design needed to be demonstrated and to also take into account the specifics of the sensor application in a hypothetical final detection device. Therefore, the focus of my work is represented by the following research question: *"What is a suitable way to design a SQUID that would be able to detect the predicted magnetic monopoles in topological insulators (mimicked by an applied external magnetic field)? What would be the further considerations in the application of a SQUID in a topological insulator device?"*; with the following subquestions:

1. Is the design of such SQUID possible and why yes/not?
2. What were the adapted methods and was it possible to fabricate SQUIDs?
(From the fabricated SQUIDs which ones are promising solutions and which ones not and why?)
3. Are there corrections or other solutions that can be adapted for better/possible designs in the future?
4. What were the encountered limitations and what are they due to?
5. What would have to be considered in a design to give possibility for the sensor to be implemented in a hypothetical topological insulator device?

Based on theoretical aspects, the current report analyzes the problems of SQUID fabrication and describes the decisions and methods adapted. A full design model was developed and the possibilities for re-design summarized. The execution of the research concerned only the available resources and facilities at the host organization.

II. Situational and Theoretical analysis

In this chapter the reader can find the initial analysis performed regarding the problems of the research and the final hypothesis for the research outcomes.

The first step in the current analysis was to investigate why SQUIDs are considered an appropriate solution and why the design of such would be appropriate for the ultimate goal of the research on topological insulators the ICE group at the University of Twente is performing, namely the detection of magnetic monopoles. As already shown by the rationale, this is important, as other solutions were already hypothesized in the scientific world. Knowing the reasons helped narrowing the current assignment and shaping a hypothesis.

In general, SQUIDs are the most sensitive magnetometers.[16, 17, 18] Therefore, they are not surprising candidates for the current project. However, as discussed in the rationale already, the magnetic force microscope (MFM) was another possibility for the detection of monopoles at the surface of topological insulators.[5, 11, 12] Nevertheless, the proposed procedure of measurement in [11] reviews the complexity of using MFM while SQUID set-ups for magnetic monopole detections stay simpler to comprehend and apply. But before comparing these methods, it is important to first understand the basics regarding the hypothesized magnetic monopoles in topological insulators and the idea for their detection, given by physicists so far. In the next discussion extensive attention will be paid to reference [5], as it is also very representative for the aims of the ICE group for the TIs research and explains in detail the physics of the magnetic monopole phenomenon.

II.I Magnetic monopoles in topological insulators

In electromagnetism theory, the method of images assumes that when point charge is brought on top of a conducting surface, it induces an image point charge below the surface.[19] Without going through the deep theoretical considerations (which can be found in [5, 11]), it is hypothesized that in TIs (which are insulating in their interior but conducting on their surface), a charge impurity close to the surface induces in a similar way a magnetic monopole. Together the system of electron (charge) and monopole is considered a dyon. Figure 2.1 provides an illustration:

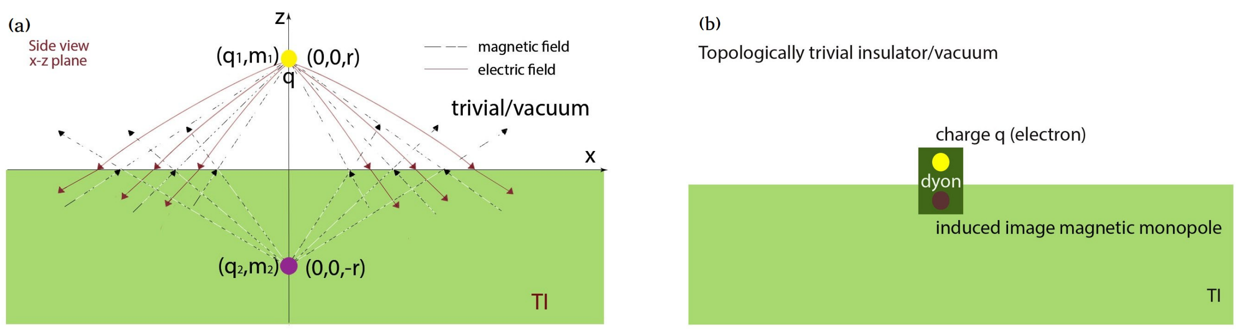

Figure 2.1: Inducing magnetic monopole in TI

(a) The lower part is represented by topological insulator (green) and the upper part by normal insulator or vacuum. An electric charge q is brought close to the surface. If viewed from below there would be image electric charge and magnetic monopole q_1 and m_1. While when viewed from above– image charge and monopole q_2 and m_2. At the limit of the electric charge being at the very surface, it is considered to form a dyon electron-monopole pair (b). Adapted from [5]

It is possible to estimate the magnetic flux due to the dyons, as explained in the same paper from which the figure is adapted.[5] The procedure includes calculation of the dyon‘s *statistical angle* φ and knowledge of the dielectric permittivity and magnetic permeability of the TI and normal insulator in the set-up of figure 2.1. The initial relation states [5]:

$$\varphi = \frac{2\alpha^2 P_3}{(\epsilon_1 + \epsilon_2)(\frac{1}{\mu_1} + \frac{1}{\mu_2}) + 4\alpha^2 P_3^2} \qquad (2.1)$$
$$\alpha = \frac{e^2}{\hbar c}$$
$$P_3 = \pm\frac{1}{2}$$

Where:
α: term describing the magneto-electric effect in the TI (the fine structure of TI)
P_3: the magneto-electric polarization in a TI (with two allowed values, depending on the direction of polarization) [1]
$\epsilon_{1,2}$: the relative permittivities of the TI and normal insulator
$\mu_{1,2}$: the relative permeabilities of the TI and normal insulator
$\hbar$: the Dirac constant $\hbar = \frac{h}{2\pi}$ with h Plank‘s constant
e: the charge of the electron
c: the speed of light

It is possible to select any of the two allowed values for P_3 as it would just affect the sign of the flux calculation. The flux, generated by the monopoles could be estimated as [5]:

$$\Phi_{monopoles} = N\varphi\Phi_0 \qquad (2.2)$$

Where:
Φ_0: the flux quantum $\Phi_0 = \frac{h}{2e} = 2.0678 \times 10^{-15} Wb$
N: the number of dyons (monopoles) $N = nS$ with n the density of dyons and S the area

Following the relations above one can tune the density of charge on top of a TI sample and perform measurements in order to track the validity of the expressions. Thus, this is the main mechanism of supplying theoretical proof for the presence of monopoles. After the current discussion (even though that the exact manner of bringing the charges on the surface of the topological insulator is not yet decided upon) the methods of measuring the field, produced by the monopoles, can now be compared.

II.II Comparison between MFM and SQUID measurement

An MFM measurement is simple to understand but complicated for analysis. The figure below gives a reasonable visualization of the MFM measurement. More on the procedure of calculation can be found in [11]. In general, the MFM tip is brought to the surface of a TI and by the force measurements performed it is possible to calculate the effects of a charge impurity at particular distance from the tip. Then after the proper analysis one can conclude if there are arguments to support the presence of image monopole.[5, 11]

[1] In normal insulator P_3 is 0, so is φ.

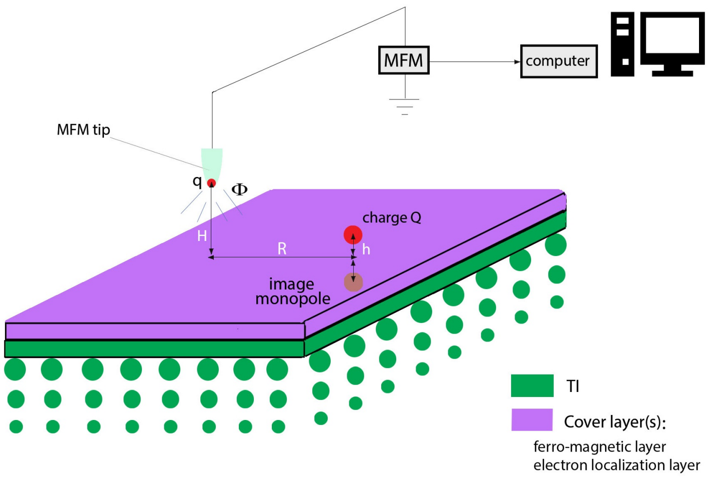

Figure 2.2: MFM scanning technique

Cover layers with charge localization and TI properties tuning function are deposited on top of TI layer. MFM tip characterized by charge q and flux Φ is moving and scanning the surface and recording the force of interaction with the sample while the distance R to deposited charge impurity Q is also known. Both the tip and the charge impurity are above the surface of the TI at known height. Image monopoles are induced below the TI surface. Statistical analysis of the measurements is used to identify the presence of monopoles. Adapted from [5, 11]

The reader can see that this strategy requires a lot of pre-setting and monitoring. Knowing the distance to a charge impurity seems to be extensive task, especially with charge densities up to $10^{11}cm^{-2}$, as proposed in [5].

This set-up already seems quite complicated compared to the SQUID set-up for measurement in which in theory a lot less setting-up and analysis needs to be performed (after the initial design and conditions of usage are known). A SQUID ring would not require information on the coordinates of the charges brought to the surface, as long as they are in the SQUID vicinity or the overall set-up geometry is known, so initial calculations could be performed. This is due to the fact that only the magnetic field passing through the sensor will be accounted for.[5, 20] The reader can find the SQUID set-up idea below.

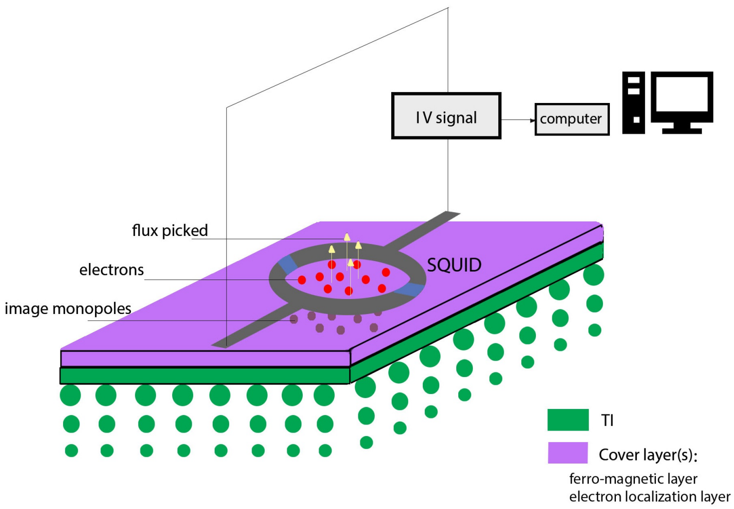

Figure 2.3: SQUID measuring technique

Cover layers with charge localization and TI properties tuning function are deposited on top of TI layer. A static SQUID is positioned on top of the system. Charge is brought to the surface. Image monopoles are induced in the TI and magnetic flux lines cross the area of the SQUID loop, producing a measurable signal. Adapted from [5]

Even if this is not exactly the setting in the final TI measuring device that would be designed in the future, a SQUID measuring mechanism reviewed itself as much more integrable approach. Additionally, once set, the SQUID read-out electronics and measurement interface would stay rather simple, as no scanning and movement would be required. There is no doubt that MFM is an applicable solution, but such microscopes provide the risk of potentially invasive action of the tip due to its stray magnetic fields, which is not desired in the current situation.[21] Critically speaking, there are also risks of choosing the SQUID as an instrument. While MFMs are rather standard and widely used machines, a SQUID sensor has not been designed and tested for the purpose currently discussed. But exactly this was going to add higher value to the current on-going research at the ICE group and therefore predefined the choice to continue further with a SQUID in this assignment.[13]

Nevertheless, it needs to be stressed that the preference of the ICE group was the strongest deciding factor. Therefore, it is recommended that after the current assignment more work is done on MFM research in order to have basis for practical comparison rather than only theoretical overview of the method.

II.III SQUID general types

After the first part of the current analysis showed great potential for the integration of SQUIDs for monopole detection in TIs, the theory of these devices was analyzed in order to build a hypothesis on the potential design results.

The structure of every SQUID includes two main building blocks: a superconducting loop and one or two weak links which interrupt the loop.[20] Together, the weak link and the superconducting material on both of its sides form a Josephson junction. SQUIDs with one Josephson junction (normally point contact) are referred to as rf SQUIDs and the ones with two junctions– dc SQUIDs. While rf SQUIDS are used to measure magnetic flux variation in time, dc SQUIDs are used as tools to measure directly the flux crossing the superconducting loop.[20]

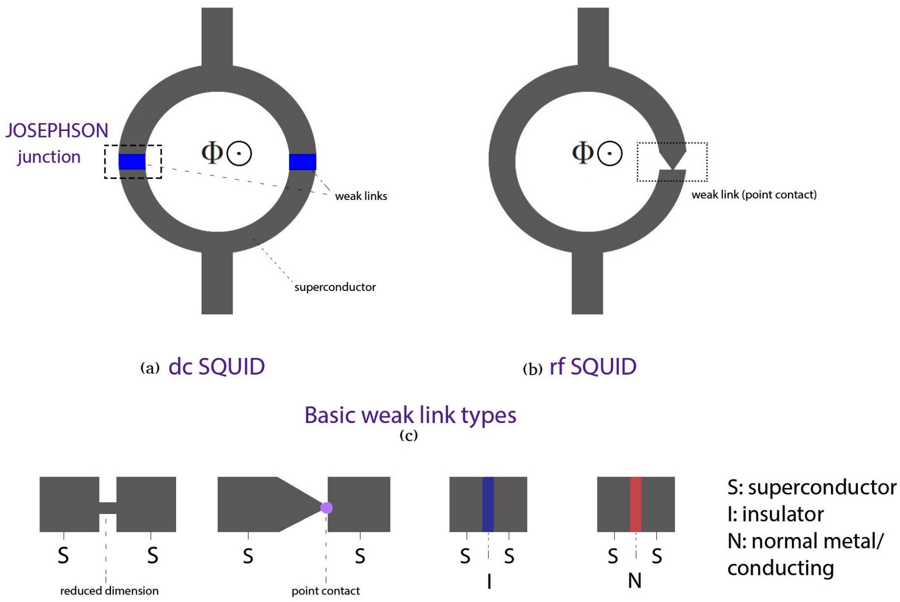

Figure 2.4: SQUID structure and types

The main two types of SQUIDs, including the basic types of weak links. SQUIDS could be manufactured in various shapes and sizes, as well as the weak links. The two general categories of SQUIDs are dc (a) and rf (b). The weak links (c) can be divided in several categories: reduced dimensionality, point contact, insulating, and conducting links. Adapted from [20]

Considering that the goal is to measure the presence of magnetic monopoles, it is already clear that a dc SQUID should be designed. Of course, when varying the amount of charge brought to the surface of a

TI, then rf system would still serve as a tool to measure the difference of the flux, produced by monopoles density change (if the charge density on the surface is altered). However, one should consider that this would be unnecessary complication of the measuring mechanism, due to the fact rf SQUIDs operation is based on hysteresis and its fine tuning.[20] Additionally, with appropriate calculations (shown later) dc SQUID could be already adjusted in a way to have enough resolution in order to produce distinguishable readings for the desired charge (monopole) density change.

II.IV dc SQUID initial design considerations

In order to create a hypothesis on the potential designs, the mechanism of dc SQUID sensing was analyzed. The main point of interest was the $I-V$ (current-voltage) characteristics of a dc SQUID, and its dependence on the magnetic flux crossing the SQUID. From the discussion of these many potential design parameters emerged.

Josephson junctions and Josephson effects

Starting from the $I-V$ characteristics, it is important to understand the nature of a Josephson junction, as the dc SQUID is in fact two junctions in parallel (as shown in figure 2.4 on page 5). When a weak link is present at the interface between two bulk superconducting wires, it would alter the circuit properties. Normally, a superconductor is characterized with zero resistance (below some critical temperature), magnetic field penetration depth (the depth to which external magnetic field could penetrate in the superconductor) and critical current which could be passed through it without destroying the superconducting state.[22] The presence of a weak link alters all these properties. Up to a particular critical bias current for the junction, no voltage will build up and the junction would act as having zero resistance, however above the critical value, voltage will build up. This is the region of interest for the design of a dc SQUID, because then this voltage will be dependent on the magnetic flux through the device.[20, 23] In the simplest case, the $I-V$ characteristics looks as shown on the figure below (a). However, to have non-hysteretic junction is not an easy task. Normally, junctions show characteristics, similar to illustration (b):

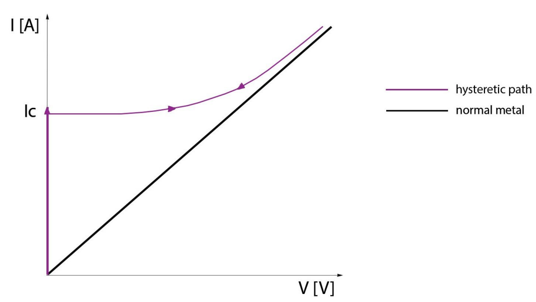

(a)

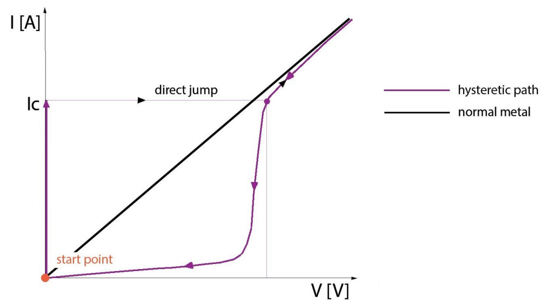

(b)

Figure 2.5: $I-V$ characteristics of non-hysteretic(a) and hysteretic (b) Josephson junction

(a): Before a particular critical current the junction is in non-voltage state. After critical current I_c is reached, voltage builds up across the junction. (b): Before particular critical current the junction is in non-voltage state. In the forward direction after critical current I_c is reached, there is sudden jump to a voltage state. If the current is reduced then, the voltage would drop slowly until the start point is reached. The characteristic is shown for temperature between $0K$ and the critical temperature for the superconducting material T_c. Purple: the Josephson junction characteristics, black: normal metal. Adapted from [20]

In the pure superconducting state (without voltage), the current is due to cooper pairs (the carriers in a superconductor), which travel through the weak link in a phenomenon known as quantum tunneling. Figure 2.4 (on page 5) already showed that weak links might even have insulating nature, however, tunneling is still possible as quantum mechanical effect.[24] In this mode, the current is given as:

$$I = I_c sin(\gamma) \tag{2.3}$$

With:
I_c: the critical current; γ: the phase difference between the superconductors on both sides of the weak link

The phase of superconductor, similar to phase of light in optics is a measure, proportional to the momentum of the superconductor cooper pairs and thus to the current flowing in a superconductor.[25] The relation of equation 2.3 is known as the *dc Josephson effect*.

On the other hand, in the voltage build up state of a Josephson junction there are two main current carriers– cooper pairs and quasi-particles (electron remains of thermally excited and broken cooper pairs). The current of cooper pairs above the critical bias is an ac current, considered as the *ac Josephson effect* (with frequency related to the voltage as about 500 $MHz/\mu V$), so on figure 2.5 (on page 6) the time averaged characteristics is shown. The ac Josephson current is given by the same relation as in equation 2.3, but in that case the phase is time-dependent quantity [20]:

$$\nu = \frac{d\gamma}{dt} = \frac{2e}{\hbar}V \tag{2.4}$$

With:
ν: the frequency; V: the Voltage

RCSJ model

It is possible to control the ac Josephson effect and as shown in the next paragraphs eliminate the hysteresis, because as the reader might have already guessed, it would not be useful to have a hysteretic junction. The current-to-voltage correspondence needs to be one-to-one and unambiguous for the later signal readings. Thus, one design consideration for the SQUID becomes clear– the $I - V$ characteristics of the sensor must not suffer from hysteresis, *i.e.* its junctions need to be non-hysteretic.

Continuing with the discussion, when represented by the RCSJ (Resistively and Capacitively Shunted Junction) model, the junction consists of resistor, capacitor and ideal junction with critical current as shown on the figure below.[20, 23, 26]

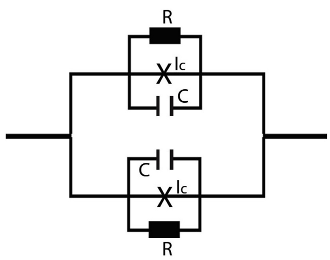

Figure 2.6: RCSJ model of Josephson junction

The Josephson junction is characterized by critical current I_C. In a circuit the junction is shunted with a resistor R and capacitor C. On the figure two junctions are in parallel as in a dc SQUID. Adapted from [26]

Here the resistance is due to the voltage build up in the junction after the critical current is reached (and the resistive shunt if additionally added), the capacitance is due to the weak link properties and the critical current I_c(equivalent for critical current density $J_c[A/cm^2]$) is specific again for the weak link. In order to keep a junction non-hysteretic we need to deal exactly with those three parameters– the capacitance, resistance and critical current. The criterion for non-hysteretic junction is given by the *McCumber parameter* in the following equation [23, 26]:

$$\beta_c = \frac{2e}{\hbar} {R_n}^2 I_c C = \frac{2e}{\hbar} R^2 I_c C \tag{2.5}$$

Where:
e: the charge of the electron
$\hbar$: the Dirac constant
R_n: the resistance of the junction in the normal state
R: the junction and shunt combined resistance
I_c: the critical current of a single Josephson junction
C: the shunt capacitance

The nature of the relation is easy to understand. When the capacitance is too high, the capacitor and resistor shunts from figure 2.6 will act as a low-pass filter and filter out the ac Josephson effect. Then the quasi-particle tunnel current would dominate. In this sense, when the voltage goes higher, more quasi-particles would tunnel and we would receive characteristic, similar to figure 2.5(b) (on page 6). This is because the electrons, being the quasi-particles need to be additionally excited to tunnel through the barrier, which happens at higher voltage. Thus, the junction would be hysteretic. On the other hand, when the capacitance and resistance of the system are low enough, then the ac effect would not be filtered out and would dominate, the tunnel current characteristic would be washed away and the junction $I - V$ plot would look a lot more similar to figure 2.5(a) (on page 6). The hysteresis will be then eliminated.

To sum up at this stage, the resistance and capacitance, as well as the critical current through the Josephson junctions of the potential SQUID were the first identified design parameters, responsible for the requirement for the SQUID to be non-hysteretic. Control over them, using the *McCumber* parameter is crucial but there is no evidence to suggest that the bi-stability problem cannot be overcomed in theory.

Dc SQUID output

In general SQUIDs are operated with a current bias slightly above the critical current to allow for a voltage build up state and then this voltage is a periodic function of the applied magnetic field. The principle output of a SQUID could be theoretically derived [20, 26] and it is predefined by the behaviour of the two Josephson junctions in parallel which build up the component. It is theoretically and experimentally postulated [20, 23, 24, 26] that the current-to-flux and voltage-to flux characteristics of a SQUID output is a rectified cosine/sine function, periodic with respect to picked magnetic flux with period of a magnetic flux quantum. Figure 2.7 (on page 9) gives an illustration of the idea of the following theoretical explanation:

The magnetic flux in a superconducting loop is quantized to integer amount of flux quanta Φ_0.[26] Therefore, there should be always integral amount of flux quanta crossing a SQUID. The limiting cases in this regard are present when the external applied flux is an integer (n) or half integer ($n+\frac{1}{2}$) value of the flux quantum. As the superconducting state appears as energetically favoured state, the behaviour of a SQUID regarding applied flux could be explained from this perspective. When integer amount n of flux quanta is applied, then higher current could flow in the sensor without dissipation. On figure 2.7 this is represented by maximal current in the device with lowest voltage output, assuming current bias higher than the critical amperage. In this case the system is in lowest energy state. In contrast, when $(n+\frac{1}{2})\Phi_0$ flux is applied, then the maximal current without dissipation in the system is lowest and the voltage at current biases higher than this critical value is highest. The system is "trying" to escape faster from the pure superconducting state without energy dissipation.[23]

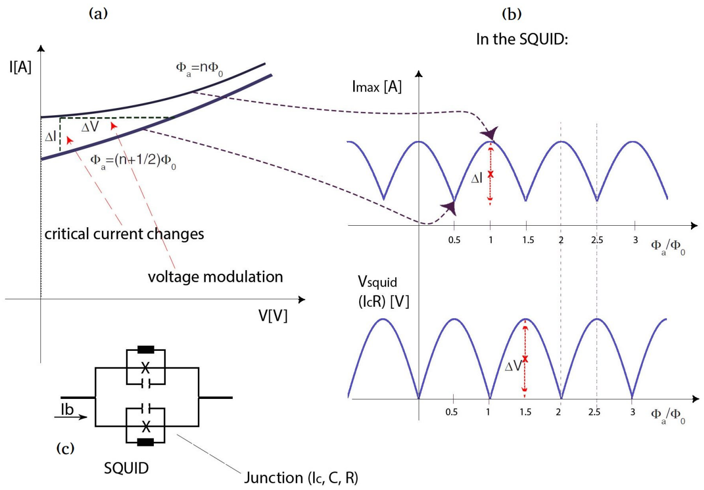

Figure 2.7: SQUID $I - V$ characteristics and output

The critical current in a SQUID and the voltage build up as affected by applied magnetic flux (a). The critical current for the junctions stay the same (c), while the SQUID shows modulation in its maximal current output (b), periodic in magnetic flux. Respectively, the voltage build up across the system is periodic in magnetic flux (b). Adapted from [24]

The modulation of the SQUID output occurs due to complicated interference processes in the loop,[23] but it is possible to explain the basics with mathematical model. While the shape of the modulation would be similar for all SQUIDs, its depth is mainly predefined by the inductance of the system, because screening current is additionally induced to compensate for the flux quantization, explained earlier.[20, 23, 24] To give more insight in the situation, we imagine a SQUID loop as on the figure below.

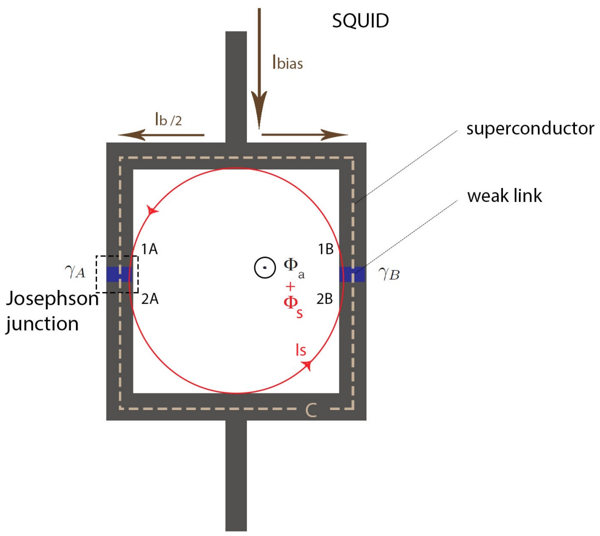

Figure 2.8: Screening of magnetic flux in a SQUID

If the SQUID system has an inductance, it screens magnetic flux. A bias current is applied to the circuit and next to it screening current flows. The screening current changes the maximal current modulation and the modulation depth of the SQUID output, giving effect also for the measured voltage modulation. Adapted from [24]

The system is biased with current I_b, which is high enough to allow for voltage state of the junctions. The Josephson relation, excluding the screening current states:

$$I_b = Ic(sin(\gamma_A) + sin(\gamma_B)) \tag{2.6}$$

Where γ_A and γ_B are the phase differences between the superconductor pieces at each junction:

$$\gamma_{A,B} = \varphi_{2A,B} - \varphi_{1A,B} \tag{2.7}$$

Considering a loop C deep inside the superconductor, we know that the current needs to be zero. This is due to the *Meissner effect* which states that the magnetic induction in a superconductor is zero, so no current should flow which could induce magnetic field.[22] We also know that the momentum of the cooper pairs in a superconductor is given by (as the momentum of light particles is given by the gradient of the phase of the wave, multiplied with $\hbar$):

$$p_{cp} = \hbar\Delta\varphi \tag{2.8}$$

When positioned in electric field, Cooper pairs will gain additional momentum [25]:

$$p_{cp_E} = -2e\boldsymbol{A} \tag{2.9}$$

Where A is the vector potential. We use twice as big charge in the equation because cooper pairs are having the charge of two electrons.

But because the current density across the contour C is zero, *i.e.* the momentum of cooper pairs is zero, then:

$$\hbar\Delta\varphi = 2e\boldsymbol{A} \tag{2.10}$$

Therefore, after applying the equation above for every phase in equation 2.7 and integration we can find out that:

$$\gamma_A - \gamma_B = 2\pi\frac{\Phi}{\Phi_0} \implies \gamma_{A,B} = \gamma_0 \pm \pi\frac{\Phi}{\Phi_0} \tag{2.11}$$

Further simplifications [20, 23] show that the maximal current through the SQUID is given by:

$$I_{max} = 2I_c cos(\pi\frac{\Phi}{\Phi_0}) \tag{2.12}$$

This is exactly the cosine periodicity shown on figure 2.7 (b) (on page 9). But now, taking into account the screening, the actual flux in the SQUID is not equal to the flux applied, but rather it is a sum of the applied and self-induced flux. From electrodynamics it is known that the screening flux is equal to the product of the SQUID inductance and some screening current ($\Phi = LI_s$). And because the screening current would be always present, the current in each junction would be equal to $I_b/2 \pm I_s$ Therefore, if one of the junction reaches its critical point, the value of the current in the other one would be smaller with twice the screening current value. Therefore the maximal current in the SQUID will never reach a depth of zero as in the inductance-free case. We therefore clearly show that the bias current and inductance of the SQUID need to be taken into account. In order to control this design issue it is important to consider the *screening parameter* [23]:

$$\beta_l = \frac{2\pi LI_c}{\Phi_0} \tag{2.13}$$

The smaller this parameter is kept in the design, the smaller the screening effect is and the measured fluctuations would be mostly due to the applied flux. By also choosing appropriate bias current in combination with inductance calculations the resolution will be improved over one period of the SQUID voltage output. The more voltage change over one period, the greater the flux per voltage output will be.[23]

Dimensions and geometry

Knowing the simple relation between magnetic field induction B and magnetic flux Φ: $\Phi = BS$ (with S the area), it is possible to calculate for a particular magnetic field strength of the hypothetically induced monopoles what the flux picked would be and from there, what area would be suitable for a SQUID in order to take full advantage from the periodicity of the output.

It was possible to perform a calculation and compare the results to the requirements of the ICE group. In reference [5] a general calculation method is postulated with which the parameters of the TI and normal insulator layers (as on figure 2.1 on page 2) could be taken into account for the derivation of the magnetic field generated by the monopoles. This procedure was already introduced in equations 2.1-2.2 (on page 3) . This method was used and the calculations are presented in chapter A of the Appendix.

It was identified that SQUIDs with radius below $10\mu m$ (or area below $100\pi\ \mu m^2$) would be able to efficiently measure the magnetic flux, created by charge carrier densities from 10^{11} to $10^{12}\ e^-/cm^2$ (respectively the same densities of $monopoles/cm^2$) and the output would be within one period of the SQUID characteristic modulation. The densities were taken as standard. After consultation with an expert from the ICE group, this result was discussed and identified as satisfactory, because there are no general practical limitations in manufacturing SQUID with such effective area.[13]

Another factor that emerged as an important variable was the SQUID shape. The component geometry would theoretically influence its inductance and from the previous sections it is clear this is issue of high priority.

Operation and Integration

A SQUID consists mainly of bulk superconductors. It is crucial to note that the temperature of operation for the system needs to be low enough, so to be between $0K$ and the critical temperature T_c for the superconducting material. A bath cryostat is available at the University, so measurements and designs could be adapted for critical temperatures down to $2K$, which relieved the concerns regarding this design parameter.

From integration point of view it was important to consider at later stages in the project what could be done to make the integration of the potential SQUID(s) in a topological insulator device optimal. As the main goal of the current project was to provide an overview of the possible designs, the application-specific problems for the sensor needed to be taken into account and provided technical discussion and testing when possible.

II.V Summary and hypothesis

SQUIDs were compared to the other strong candidate for the detection of magnetic monopoles– namely the MFM strategy of measurement. The SQUID technique showed itself as more desirable and mobile approach. Several design considerations and parameters were identified and analyzed. The design and manufacturing of the hypothetical dc SQUID(s) showed to require many steps with the intention of controlling the resistance, capacitance, critical current and inductance of the sensor in order to have desired output. However, no general theoretical limitations are present when trying to control these factors. Calculations were performed on the hypothetical size which also did not give any concern on the possibilities of manufacturing.

Therefore, it could be hypothesized that a SQUID design for magnetic monopole detection is possible when considering the parameters above. From theoretical perspective there were no factors suggesting the inability of a SQUID to perform in a topological insulator device.

III. Conceptual Model

In this chapter the reader finds the discussion on the design factors and analysis on which ones were of greater/minor importance for the dc SQUID design for detection of magnetic monopoles in TIs. The table below describes the parameters and factors identified in the prior chapter. In the remarks the reader can find as well the initial considerations regarding the control over those factors. In the following text reference will be made to each of the parameters in the table.

Parameter	**Desired value/situation**	**Relevant to**	**Remarks**
1.Operational temperature	Below T_c	Josephson junction	Temperatures as low as $2K$ are possible at the bath cryostat
2.Size (and Shape)	Area below $100\pi\ \mu m^2$/ radius below $10\mu m$	SQUID	SQUIDs with such size of the loop can fabricated
3.Non-hysteretic sensor	$\beta_c << 1$	Josephson junction	Adjust β_c parameter via shunt resistor and capacitor
4.Inductance	β_l as small as possible	SQUID	Adjust SQUID geometry to account for the size and inductance requirement
5.Critical and bias currents	Dependent on fabrication phase	Josephson junction, SQUID	Adjust critical current in fabrication phase in order to later know with what bias current to work
6.Integrability	As scalable as possible	SQUID	In final design make account for the difficulties of positioning the SQUID over TI device.

Table 3.1: Identified design parameters and considerations regarding their control.

III.I Operational temperature

Starting from parameter 1, the operational temperature, it is important to note down that low temperature is needed not only to keep the superconducting state of the material (for Niobium for example, superconductivity appears below $9.2K$ [22]). Low temperature suggests low thermal noise. Additionally, for a Josephson junction to operate accordingly and for the Josephson effect to be present we define the *relevant* temperature, above which the Josephson effect cannot be observed and the junction would act as nearly normal and would be most surely hysteretic.[20] This temperature is in fact directly connected to the expression for the energy of the Josephson junction (therefore also to the Josephson coupling energy, the energy needed to advance the phase difference across the junction from 0 to π).[23]:

$$U_J = \int_0^t IV dt = \frac{\Phi_0 I_c}{2\pi}\int_{\varphi_0}^{\varphi} sin(\varphi)\frac{d\varphi}{dt}dt \tag{3.1}$$
$$U_J = E_J(1 - cos(\varphi))$$
$$\implies E_J = \frac{\Phi_0 I_c}{2\pi} = \frac{\hbar I_c}{2e} = k_B T_J$$

With E_J the Josephson coupling energy

From here, we derive the *relevant* temperature T_J:

$$T_J = \frac{\hbar I_c}{k_B 2e} \tag{3.2}$$

With k_B the Boltzman constant and the remaining notation as used earlier in the paper.

For this temperature, the thermal energy of the system will be enough to advance the phase difference across the junction from 0 to π, and therefore the dissipation-less current cannot be observed, as its appearance is governed by exactly the junction ability to adjust its phase difference and stay in preferred low-energy state. The ac Josephson current will not be observed either, as then the phase is not varying in time. One can also expect that for temperature close to this value, the junctions $I - V$ characteristics will be also distorted.[20]

When considering all this, it is a lot more clear why the temperature is crucial. It will in fact determine the limit for the critical current we can use before the Josephson effect is washed away. We would like the thermal energy of the system to be a lot lower than the Josephson coupling energy, so not to risk to operate at a boundary. That is why we define another parameter Γ which will help keeping track of the relations above:

$$k_B T << \frac{\hbar I_c}{2e},\ \Gamma = \frac{2\pi k_B T}{I_c \Phi_0} << 1 \tag{3.3}$$

To summarize, the temperature is a factor that is crucial and luckily adjustable in a bath cryostat. By making sure that the Γ coefficient is well below 1 we could be reassured that the Josephson effect would not be eliminated.

III.II SQUID size

Parameter 2 from table 3.1 (on page 12) is the SQUID size. Calculations were already performed in the previous chapter of the report to identify that sensors with area less than $100\pi\ \mu m^2$ would be suitable to detect monopoles with density between 10^{11} and 10^{12} $monopoles/cm^2$. Please refer to chapter A of the Appendix and equations 2.1-2.2 (on page 3) for more details.

Here it is important to discuss and clarify the importance of the area as factor. First of all, it needs to be noted that the area that is being discussed is the SQUID sensor *effective* flux-picking area. Thus, the calculations performed would not be in perfect accordance. In most cases, the ratio between the effective and geometric SQUID area would be in the order of unity, but it should be considered that due to the *Meissner* effect the loop would be practically enlarged. This is because magnetic field lines, trying to go through the actual superconductor would be bent and still sent through the loop vicinity. Moreover, as for the inductance, one can imagine that the shape and sensor geometry would also have effect on the effective area. Conical SQUIDs would channel magnetic flux better than flat ones and then the actual effective area might turn out to be a lot bigger than the geometric one. Thus, the actual SQUID size problem can be first approached from shape perspective. Until the geometry of the sensor stays undefined, the size and (later) the inductance calculations would become too generalized. That is why it was crucial to decide on particular shapes at first.

After a conversation with a technical expert [27] it was discovered that fabrication of SQUIDs with washer shape is a lot faster than fabrication of circular loops. Thus, considering the timeline of the project the washer option was then chosen for the current assignment. This eliminated the shape as a design parameter. However, no statement is made here that circular SQUIDs would or would not serve as well as magnetic monopole sensors. Furthermore, knowing the selected shape more research was performed on the effective area and sizes. For a square washer, the effective area is dependent on the inner and outer dimension, as given below [28]:

$$A_{eff} = \alpha H h \tag{3.4}$$

With:
α: coefficient of order unity
H: Outer dimension
h: Inner dimension

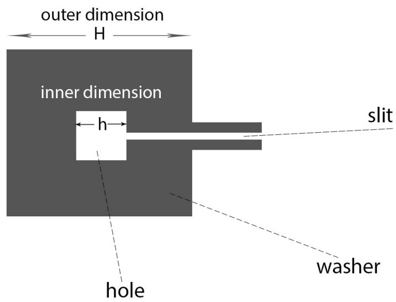

Figure 3.1: SQUID square washer with characteristic dimensions

The characteristic outer and inner dimension of a square washer shaped SQUID. $H-$ outer dimension, h-inner hole dimension. Adapted from [28]

It is important to state that the current relation would work only if the outer dimension is at least 3 times bigger than the inner dimension [28]. That is why the limit of validity for this formula would be if the SQUID width (width of superconducting wire) is actually equal to the dimension h. For the constant α the literature suggests order of unity [28, 29]. Thus, it should be kept as consideration but it is not a parameter which deserves too much attention. Sensors can be fabricated in batches with varying geometry and slight size differences in order to account for such uncertainties.

In summary, size is an important factor which can not be neglected. The shape of the SQUID however was not further investigated in this project as the washer geometry was already selected.

III.III Non-hysteretic sensor

In the previous chapter a lot was discussed on hysteresis. Here we focus on the means of how to control the problem. Hysteresis might appear in the Josephson junctions, building up the sensor. The bi-stability of the junctions is controlled by the β_c (*McCumber*) parameter, introduced in equation 2.5. As the reader can already see, several are the important factors to eliminate hysteresis (resistance, capacitance, critical current). Hysteresis might appear for values well above 1 [30], but to reduce risks it is smart to aim for solid grounds and keep it well below 1. There exists strong correlation between the β_c and Γ parameter from equations 2.13 and 3.3 (on pages 10 and 13). As already discussed in the situational and theoretical analysis, hysteresis would appear when the ac Josephson effect is inhibited [20] and this might happen for high values of both two parameters mentioned above. Keeping them low is then more reasonable and safe rather than taking a risk.

Further on, this was the moment to account for the material that would constitute the weak links, as the junction itself would possess capacitance. Then actual shunt capacitor might not even be needed, which would en-ease the fabrication process.[27] Weak links can be prepared from various types of materials, but because the link dimensions can be adjusted to yield the desired capacitance, it is not needed to consider this as major issue. It is possible to lay aluminum layer of several nanometers and fabricate weak links of desired area.[27] Oxidizing part of the aluminum layer then provides a dielectric layer for a *SNINS-type*(superconducting-normal-insulating-normal-superconducting) Josephson junction. For the superconducting material, considering that low temperature operation is anyway advantageous for the system (see the operational temperature discussion from earlier), we are free to use Niobium (Nb) with critical temperature $T_{CNb} = 9.2K$.[22] The selection of $Nb/AlO_x/Nb$ type of Josephson junction is not uncommon and the majority of SQUIDs in the recent decades with various applications have the current configuration.[31] Calculations could be then easily made on the capacitance and size of the weak links which later could be incorporated in a Josephson junction. More on the fabrication plans is available in the Research Design section of this report. Here we provide a basic calculation for a several nanometers thick layer of AlO_x and area of several micrometers parallel plate capacitor:

$$C_{wl} = \frac{\epsilon\epsilon_0 A}{d} \tag{3.5}$$

Where: C_{wl}: the capacitance of the weak link
A: the area
ϵ: the dielectric constant (in this case of AlO_x)
ϵ_0: the dielectric permittivity of vacuum ($\epsilon_0 = 8.854 \times 10^{-12} F/m$)

The dielectric constant of aluminum oxide thin layer was taken as ≈ 10, as literature proposes different values ranging from 7 to 11, due to the different concentrations of aluminum oxides and their ratio.[32, 33] Thus for an area of $6\mu m^2$ and thickness of $1nm$ one would receive $\approx 0.6pF$. This is a small enough capacitance, in the order of the ones already reported as reasonable and used.[27, 34] By reducing the area and/or increasing the thickness we can tune the capacitance to even lower values and further reduce the β_c coefficient from equation 2.5. Additionally, since it depends on the oxidation time and conditions for the aluminum layer what its properties (thickness, dielectric constant) will be, one can adjust further the capacitance via testing.

The other variables in the β_c parameter are the shunt resistance and the critical current. While the shunt resistance can be fabricated from metals with known conductivity and adjustable dimensions, the critical current is a more complicated task. The oxidation of the deposited Al layer is crucial for its tuning (also for the capacitance) and that is why testing had to be performed in order to observe the relation between critical current and oxidation conditions. There are previous documented procedures on the relation between oxidation time and the junction capacitance and critical current at the University of Twente [27], but due to their dating it was needed to perform experiments again.

It is clear from the discussion above that the resistance, capacitance and critical current are not design factors that can be neglected, but luckily are adjustable variables.

III.IV Inductance

The SQUID inductance is one of the following identified design parameters from table 3.1 (on page 12). As already discussed, the inductance of the system would affect the sensor critical current modulation and respectively its output voltage modulation. Therefore this would directly influence the resolution as the voltage per unit flux change would be affected. Additionally, it was identified that the inductance is directly connected to the *screening* parameter β_l from equation 2.13. Keeping this parameter low would result in smaller effect on the sensor output modulation.[23]

In order to be critical and analyze the importance of the inductance, calculation needed to be performed. For the selected SQUID shape and for the considerations on the size, the inductance of the system was estimated and discussed. The reader can find the calculations in the following paragraphs. Three different inductance contributions can be distinguished for washer-shaped SQUID [28]:

- Inductance due to the flux-picking hole
- Slit inductance
- Kinetic inductance

The relations used to calculate the inductive contributions are given in [28]:

$$L_{hole} = 1.25\mu_0 h \quad (3.6)$$

$$L_{slit} = 0.4\frac{K(k)}{K`(k)}10^{-6}l_{slit}$$

$$L_{kin} = 1.25.10^{-6}\frac{\lambda^2}{d}\frac{2l}{w}$$

With:
μ_0: the magnetic permeability of vacuum ($\mu_0 = 1.257 \times 10{-}6H/m$)
$k = \frac{s}{s+2w}$
$\frac{K(k)}{K`(k)} = \left[\frac{1}{\pi}ln\left(2\frac{1+\sqrt{k_c}}{1-\sqrt{k_c}}\right)\right]^{-1}$
$k_c = \sqrt{(1-k_c^2)}$

The figure below gives an overview of the dimensions used in the equations:

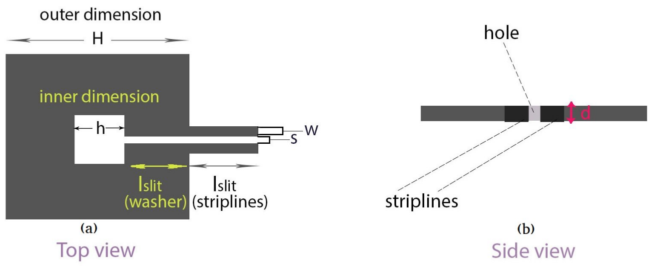

Figure 3.2: SQUID dimensions contributing to its inductance

The characteristic dimensions of square washer SQUID, playing a role in the calculation of its geometric and kinetic inductance. (a): Top view of the structure with identified washer, hole and slit dimensions and (b): side view from the right of the structure with identified thickness. Adapted from [28]

For the derived SQUID size approximation the following table was prepared, including example dimensions and calculated inductances:

Quantity	Calculated/Known
Washer outer dimension H $[\mu m]$	30
Washer inner dimension h $[\mu m]$	10
A_{eff} $[\mu m^2] \approx$	300
Slit width s $[\mu m]$	2
Strips width w $[\mu m]$	3
Washer/Strips height $[nm]$	150
λ Nb $[nm]$	≈39 [35]
L_{hole} $[pH]$	15.7
$L_{slit\ in\ washer}$ $[pH]$	4.82
$L_{slit\ outside\ washer}$ $[pH/\mu m]$	0.72
$L_{kin\ striplines}$ $[pH/\mu m]$	0.01
$L_{kin\ washer}$ $[pH/\mu m]$	0.002

Table 3.2: Adapted calculation of SQUID inductances based on example dimensions

There are two slit inductances contributing, from the slit in the washer and the slit outside. The dimensions chosen for the washer size were justified earlier and the remaining example dimensions were discussed on a meeting with an expert as reasonable (possible to realize in the lab facilities).[27]

The kinetic inductances show as negligible, compared to the slit inductances, and were further omitted because their estimation in the design might become less significant than the certainty that can be achieved. From the table it is visible that the inductance of a hypothetical SQUID with the suggested dimensions would be in the range of tens of pH. In such case, when trying to adjust the *screening* parameter β_l (equation 2.13 on page 10) to low value, for example 1, then the critical current would be in the range of tens of amperes. When looking at an old (unpublished) documentation at the ICE group archives [36] critical currents of this range were recorded in $Nb/AlO_x/Nb$ junctions in which the aluminum layer was partially oxidized. A scanned graph from this archive could be found in Appendix B. In their model, the researchers have used similar set-up, as in our calculations [36] (thickness of Nb layer of $150nm$, thickness of Al layer less than $10nm$, giving only several nm thick Josephson junction dielectric layer, as used in the capacitance calculations in the previous section). Thus, it was expected that for the new design similar results could be achieved. In any case, trying to reduce the inductance as much as possible stays a must and from our current discussion it is visible that in the range of pH and with tuning the critical current of the junctions we could even aim for β_l as low as 1.

III.V Critical and bias currents

From the previous sections it is clear that there are several currents important to discuss:

- The critical current of the Josephson junction(s) I_c
- The critical current in the SQUID I_{cSQUID}
- The bias current with which the SQUID is operated

In the previous discussion on the Γ, β_c and β_l parameters we see that the Josephson junctions critical current plays an important role and will impose limitations in tuning these to the proposed in literature low values.[20, 23] That is why this current is an important design parameter. Unfortunately, without testing more practical considerations could not be done, as the conditions at the very laboratory might play an unexpected role. There are even cases of having different critical current results when oxidation of the Al layer of the Josephson junction is performed in different laboratories.[27]

As for the critical current of the SQUID, it was not possible to set this quantity in the design phase. Only after setting the Josephson junction critical value it would be possible to estimate the sensor maximal current density and its modulation, as then the inductance will start playing a role. Therefore, the bias current of the SQUID would become clear even later. Thus, the last two currents in consideration are not part of the design and could be only adjusted after direct testing and measurement on junctions and SQUIDs. However, it is clear that the critical current in the SQUID will be reduced by twice the value of the screening current $I_s = \Phi_0/2L$ and the bias current will have to be tuned slightly above I_{cSQUID}, to a value at which the SQUID read out shows maximal voltage modulation (resolution).[20, 24]

III.VI Integrability

The last identified parameter after the theoretical analysis is the integrability of the SQUID design. In order to make the sensor easier to implement in a TI device, it is important to realize that the connections and substrate for the sensor need to be also designed in a clever way, so to be easily attached to the magnetic monopole detection system.

At this stage of the research it is not important or possible to estimate with certainty the final dimensions and technology of positioning as the TI device is also still in the design phase.

Currently several ideas emerge:

- To possibly adapt the usage of transparent substrates in order to have control over the position of the SQUID in TI device (if the sensor is flipped on top of he TI sample)
- To consider fabrication of the full device on the same substrate
- To leave long pathways in order to have the sensor connection further from the detection area which will be helpful in all cases of integration

III.VII Additional

So far the focus in the report was concentrated around the very SQUID-specific design parameters. However, it is crucial to realize that there are more aspects in modeling the current research. As long as there is no actual TI device available, the monopole field had to be generated externally. To make this possible, testing had to be performed with external source which had to simulate the flux.

III.VIII Summarized concept

At the end of all discussion in the current chapter it became clear which parameters in the design could be controlled and which required more practical investigation. While crucial for the design, some quantities could not be considered without direct measurement or just simply had lower priority due to their dependence on other factors.

Here a diagram is provided, summarizing the discussion. All design problems are interconnected and their strong relationship with the limiting parameters marked.

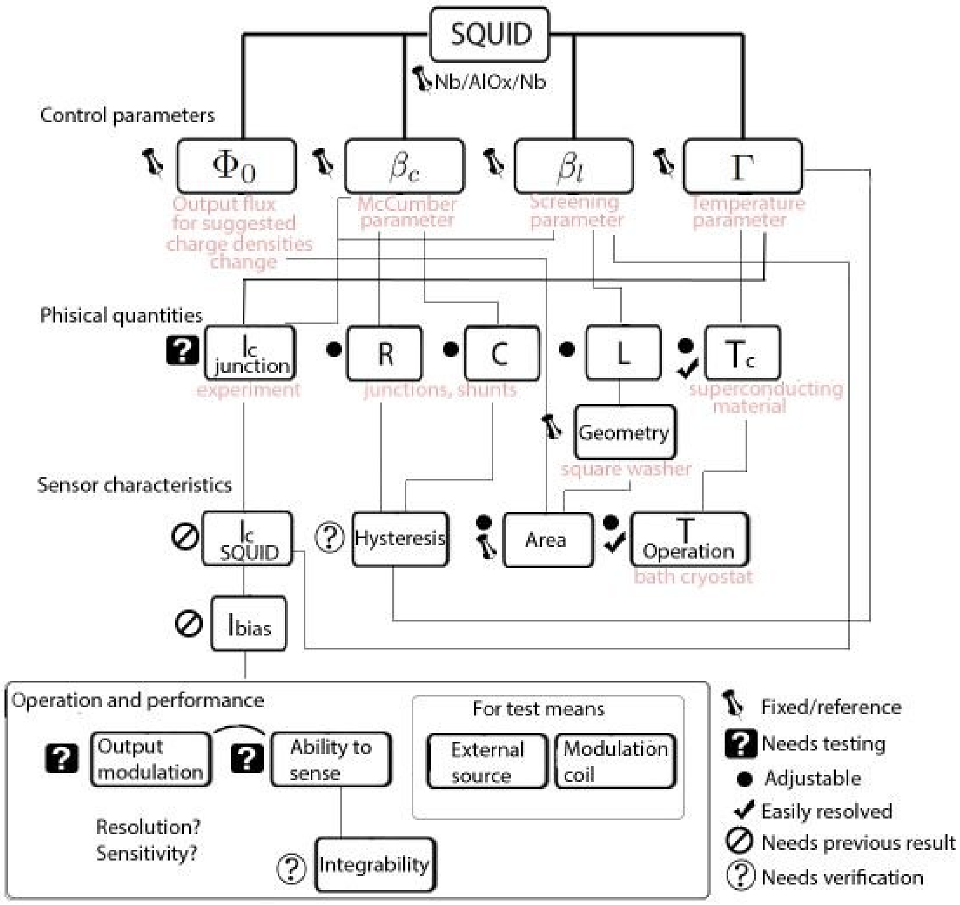

Figure 3.3: Concept summary diagram

The design parameters and the basic relationship between them.

The model of the current problem includes several steps. Even though the parameters are interconnected, some compromise can be made. The main goal was to first work on the critical current I_c problem (more precisely, current density J_c) and see what dependence can be drawn for it in respect to the oxidation time and pressure for the Al weak link. Secondly, by series of tests and measurements the β_c parameter could be adjusted. By varying the junctions size one could also adjust the capacitance, and by putting shunt resistors– the resistance of the system. For the Γ parameter not much could be done. Keeping the system at bath cryostat at temperatures below $9.2K$ (T_c for Nb) is already theoretically having big contribution, as Γ is directly proportional to temperature. At the end the SQUID(s) (with sizes of the range used in the calculations, but also possibly adding some variation) could be tested as full systems to check for potentially successful combinations of size and the rest of the control parameters. Appendix C demonstrates an example model for the design, including numerical predictions that were estimated on pre-execution basis from the literature values we already encountered in the report.

The next chapter gives overview on the approaches taken to address this model in the most efficient way.

IV. Research Design

This chapter provides overview of the execution of the research. The objectives, approaches and encountered limitations are summarized, and the decisions taken are discussed.

IV.I Fabrication

To evaluate the SQUIDs for the purpose of monopole detection, the procedure for their fabrication had to be established. The decision was made to use the ideas of the fabrication procedures known in the ICE group from before [36] and alter them, taking into consideration the new available techniques, resources and practice in the ICE laboratories (including the new records of machine usage in the labs). This was needed, as in the past different chemicals were in use, and the SQUIDs were of different loop size. Still, the same $Nb/Al/AlO_x/Al/Nb$ technology was implemented, due to the availability of the materials and due to the presence of experts to support the process.

The fabrication of junctions and SQUIDs can be described as layering the desired materials by depositing them on a substrate (Si/SiO_2) and patterning, using lithography techniques. At first, a lot of the old methods were adapted, but in the run of the testing process the procedures durations were altered (calibrated). The process always has two phases: subtractive and additive. In the subtractive phase we start with all metallic layers everywhere on the substrate and then forming the desired structures with etching. The additive process following is represented by adding new layers and shaping them in the desired form by defining the places of contact with the structures we already have. Deposition of materials was performed in two sputtering systems: Nordiko 2000 (trilayer $Nb/Al/AlO_x/Al/Nb$, Pd which was selected for resistor layers) and Perkin-Elmer 2400 (SiO_2 layers for insulation). Patterning was done by photo lithography: applying photoresist (positive, OIR 906-12 [37]), exposing to UV light under a mask of desired pattern, removing the exposed photoresist, performing desired procedures, such as etching or more deposition, and removing afterwards the remaining unexposed photoresist. This step was repeated for different masks until the layers were shaped in the desired manner, similar to electrical PCB fabrication. In the patterning process, etching and removal of parts of the deposited layers happened in three ways: wet etching with OPD developer [38] to remove exposed photoresist, Al and AlO_x; acetone etch for the removal of unexposed photoresist; reactive ion etching (RIE) with SF_6 plasma to remove Nb in a RIE etch systems; One should also distinguish between an etch, lift-off and self-aligned mask: The etch masks used protected layers under unexposed photoresist against etching procedures. Exposed photoresist was removed with OPD, etching performed and unexposed photoresist was removed with acetone; Lift-off masks were used when a material needed to be deposited at a place of exposed photoresist. Therefore after lithography, the exposed photoresist was removed with OPD, top layer deposited and then unexposed photoresist removed with acetone to lift-off the undesired part of the new layer; A self-aligned mask was also used. In that case, it combined both the function of etch and lift-off mask; As the reader can already notice, the fabrication process was quite lengthy. Therefore, it was mainly performed with 2-inch silicon wafers, which can accommodate many samples at once. Therefore, the masks used were also patterned with many junction and SQUID structures. Below the reader can find brief summary of the fabrication steps and the adjustments and calibrations performed. Appendix D gives full overview of all procedures of fabrication, including the masks, the adjustments made and the facilities used.

1. Trilayer deposition (with oxidation of part of the Al layer)
The junction trilayer was always deposited first as follows: bottom Nb($150nm$), Al($5nm$, oxidizing top $1-2nm$), Al($5nm$), top Nb($150nm$). It was important to have Al layers at the interface with Nb, so to keep the AlO_x away and not oxidize the Nb. When we keep the superconducting material as pure as possible, this will give protection against unexpected behaviour and the weak link tunnel barrier well defined. Therefore, if the sample could not be processed further directly, it was also covered with capping layer of Al. Oxidation was performed for 1h and different pressure per wafer (range: 0.1-10mbar) in the loadlock of the Nordiko system.

2. Lithography with trilayer etch Mask (Mask 1)
   To adjust the procedure, tests were performed on small samples and wafers and this is shown in entries 4, 6.B and 8.H from Appendix D. At first work was done only on small samples (entry 4) on which we tried to pattern several Josephson junctions. After succeeding, the procedure was also adjusted for wafers. The photoresist application was judged visually, as well as the quality of the patterns after exposure and OPD development (removing of exposed photoresist). The exposure time was increased from the initial 3 to $6s$ in order to be sure that the exposed photoresist will be well removed before the etching step. Those adjustments were kept for all lithographies in later steps.

3. Etching trilayer with RIE (Nb) and OPD wet etch (Al compounds)
   At first the top part of the Nb in the trilayer was etched with RIE, then the Al-based weak link layer removed with OPD, and the bottom Nb removed again with RIE. Appendix D entries 6-9 show the development on the problems of adjusting those procedures. At this stage mostly the processing of wafers was stopped and the etching tested with metallic layers on glass plates. As a result of those tests, the initial used power and timing of etching were increased. Wafers were etched for $12min$ in the RIE machine with power of $150W$. Short ($2min$, $15W$) argon pre-etch was also added. As Ar is not selective to Nb only, longer time was not suitable for the next Nb etching performed (later in the list sequence). The initial OPD concentration was reduced (from concentrated to 1:5 ratio with DI water). This was done to make sure that the solution will be less aggressive to the Al layers and avoid lateral etching of the Al layers intended to stay within the structures. The timing of the OPD etching was increased (due to the very low concentration) and Al compounds etched for $2min$ and $15sec$. This adjustment did not concern the Al capping layers, which were very thin and easily dissolved after exposed photoresist is removed during lithography.

4. Lithography with junctions etch mask, which is also the first insulation layer lift-off mask– self-aligned mask (Mask 2)

5. Etching top Nb with RIE, deposition of insulation and lift-off
   After this step the SQUID and junctions are defined:
   - Junctions are in trilayer form
   - Remaining SQUID structure is only in bottom Nb form (covered by Al/AlO_x for protection)
   - The structures have insulation around their edges

6. Lithography with second insulation layer lift-off mask (Mask 3)

7. Deposition of insulation layer and lift off
   This step increased the height of insulation around the devices. After this step the intended height is in the range of $300nm$. Mask 2 and 3 are also needed to define the effective shape and size of the junctions (receiving square junction by overlapping two different rectangles where insulation is not deposited).

8. Lithography with top Nb counter electrode lift-off mask (Mask 4)

9. Deposition of Nb and lift-off
   The Nb layer has a thickness $350nm$ and has to extend on top of the insulation. The top Nb layer also patterns the SQUID field modulation coil. Due to reasons explained later, the coils fabricated on the SQUIDs were not used.

10. Lithography with resistor lift-off mask (Mask 5)

11. Deposition of resistor layer and lift-off
    The resistor layer is approximately $75nm$ thick. Resistors were several μm wide (2-4 μm) and approximately 12 μm long. [1] Knowing the sheet resistance of Pd ($75nm$ layer has sheet resistance of $\approx 1\Omega$ [39]), the estimated resistance is $\approx 6\Omega$. Therefore the resistance is kept to be several Ohms only to keep the β_c parameter low and still damp the system. A resistor is also added between the junctions in order to stabilize the system against oscillations. At the end of this step the devices are fully defined:
    - Top electrode connection is provided for the junctions

[1] On the mask there were also shorter resistors, but they were intended for PdAu layer, which was planned for the future testing after the current assignment.

- The junctions are now damped

The figure below describes the resulting device [2]:

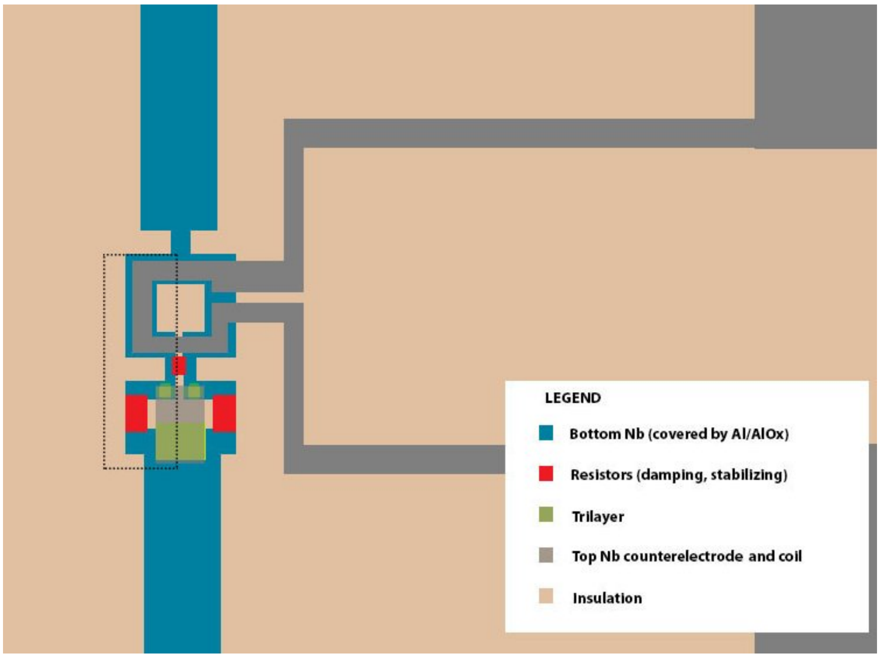

(a)

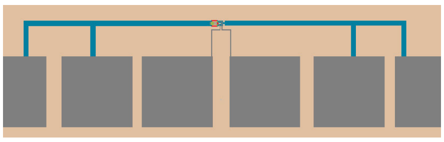

(b)

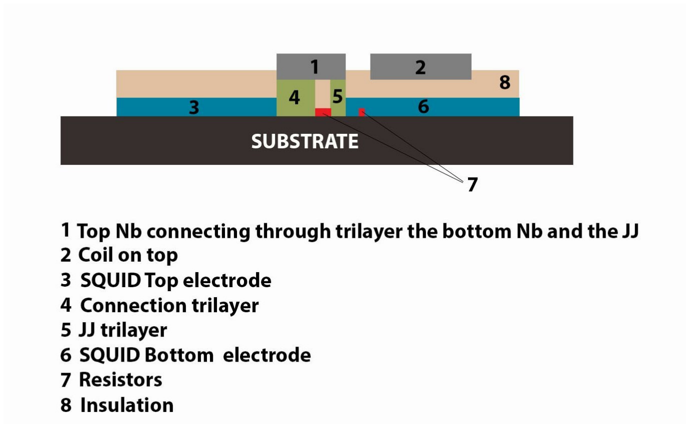

(c)

Figure 4.1: Designed SQUID devices.

(a) Top view of the intended device with focus on the SQUID washer: The SQUID is in bottom Nb form, covered by weak link remains after the etching. The junctions are in trilayer form, connected to the top Nb layer. The lower SQUID extension serves as top electrode, the other– as bottom. The interconnection between the top Nb and and the lower SQUID extension is provided by a trilayer region; Resistors shunt the junctions by connecting the SQUID electrodes (also stabilizing resistance across the washer slit). The top Nb layer is also patterned to provide modulation coil on top of the SQUID washer; (b) Top view of the overall SQUID structure; (c) Side view of the marked with dotted line area in (a): Side view provides better overview of the interconnections explained. The dimensions ratio is not to scale, but provides the right spatial distribution. JJ stands for Josephson junction;
** The interconnection (4) from (c), as the big contact pads are in fact in trilayer form. This gives no effect on the system, because their effective area is big enough to saturate any junction behaviour.

[2]The color code used here and in Appendix D for describing the devices is different. The reader is advised to always follow the legend carefully. The level of detailing in the explanation is also different here and in other figures. In the appendix all layers are accounted for.

IV.II Josephson junctions and SQUID design iterations

To address all problems of the model that was developed for this project, the process of fabrication was optimized in a way to provide information for all variable parameters and sub-goals. To observe the effects of the weak links properties, wafers with different initial oxidation were planned. A lot of dimensional variation was given for the SQUIDs on the masks, so a second iteration of calculations and mask fabrication was not needed. Per silicon wafer, a total of 126 SQUID structures were fabricated, with (inner) loop areas, varying form 40 to 260 μm^2 (all in the range of the calculations in Appendix A, considering the washer geometry area formula in equation 3.4 on page 14). For those SQUIDs the slit and junctions sizes were also varied, kept in the range of several μm, as in the initial design calculations provided in this report (Appendix C). As there can be only one thickness of resistor layer deposited when working with the full wafer, SQUIDs with the same parameters of the loop and junctions have clones with three different resistor widths. More can be found under Appendix D.

With these variations taken into account, the research process followed the steps below:

1. Fabrication of wafers with different oxidation conditions
2. Cutting the wafers
3. Selecting the structures to measure
4. Wire bonding
5. Measurement of the outcomes
6. Evaluating the results with respect to the reference parameters mentioned in the model
7. Identifying what can be changed in the fabrication in order to improve the results

As Appendix C already showed, calculations can never be precisely performed, as there will be always room for errors. One can never be sure what inductance to consider in the calculations or what exactly the thickness of the oxidized Al will be. Therefore, the current method of work was actually suitable compromise for this project. It provided many advantages with respect to single sample processing:

- Providing many samples at the end of the fabrication
- Less susceptible to damage
- Higher chance of obtaining non-defected samples
- Easier to transport

The wafers have a lot bigger surface area as compared to small samples. Therefore, many of the procedures inhomogeneities became visible. This on its own provided advantages in the sense of documenting these procedure flaws, identifying ways to fix them and in general receiving more knowledge of the processes.

IV.III Major challenges

The main challenge encountered was the calibration of the old procedures for etching. Many tests were performed to adjust the parameters of the wet and reactive ion etching, next to the running wafer fabrication. Additionally, it was discovered that the RIE process leads to substrate overetching at step 3 of the fabrication list. It was also suspected that on some samples an additional material was deposited while being in the RIE machine chamber. These were however issues that were not investigated further. Considerable attention was paid to summarize all possible recommendations and ideas on the further improvement of the research design and the adjusting of the procedures which were not (fully) resolved within the current work. Nevertheless, the research design here was fully executed and all of its steps evaluated accordingly.

V. Results

This chapter provides the results obtained regarding the procedures calibrations and the performed SQUID measurements.

V.I Samples processing

In total there were several small samples and eight wafers which started fabrication. From those, two small samples and three wafers were processed completely to be measured. The figure below gives overview of the process history per sample. For the full history of processing Appendix D can be checked, where also the samples used for adjusting the procedures are discussed.

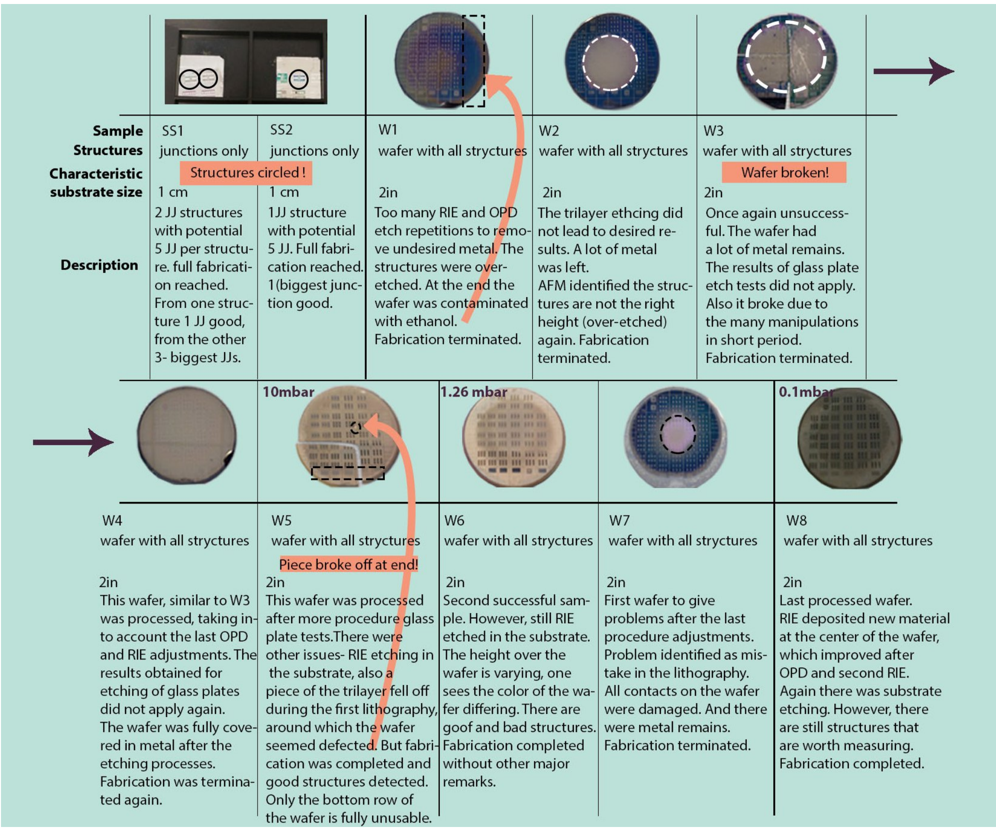

Figure 5.1: Processed samples.

Overview of the samples, milestones of the fabrication process. In total three wafers with different oxidation conditions (pressures given next to the wafers: 10mbar, 1mbar, 0.1mbar; for 1h) went through full fabrication. These are going to be the measurands of the fore-coming structures evaluations. On the figure the following short markers are used: SS– small sample, W– wafer, JJ– Josephson junction; The characteristic dimension for the first samples refer to their side, for the wafers– to their diameter. All major areas of interest or defects are marked on the images.

The small junctions samples are the only small samples that were processed for measurements. It is visible that they are the ones with the least fabrication issues. When the processing of the wafers started the problems with the procedures appeared. However, processing did not go back to small samples, as the fabrication rate was going to be too slow and there was no guarantee for the structures to be always as easy to prepare. Additionally, in some of the machines more than one wafer at a time could be processed (Perkin-Elmer). This optimized the process even more with respect to duration. On the wafers there were a lot of SQUIDs and respectively junctions and the chance of having good structures was higher. Entry 12(B, E) and 13.B from Appendix D contain records with links to microscope images taken for wafers 5, 6 and 8 which are the three wafers from where structures were measured. As expected, there were damaged, but also good-looking structures. Appendix E provides some examples.

While for wafers 5 and 6 the RIE process led to inhomogeneous etching in the substrate, for wafer 8 there were suspicions that some material was deposited in the center of the wafer, because after the second RIE (Mask 2) the center of the wafer was improved, most likely due to the lithography manipulations and the Ar etch at the beginning of the RIE. Both the substrate etching and the deposition of material were undesired processes which influenced the height distribution over the samples. It is also visible on figure 5.1 (on page 24)– the colors are not solid and change over the area. This poses an expectation that the structures might have issues at the bulk but this is deviation that could not be overcomed at this stage.

V.II Measurements

Measurement set-up

Measurements of devices were performed at a bath cryostat at $4.2K$– well below the critical temperature of Nb ($9.2K$ [22]). Samples were always provided two sets of connections (for current and voltage signal). The diagram below provides the principle schematic for the performed measurements.

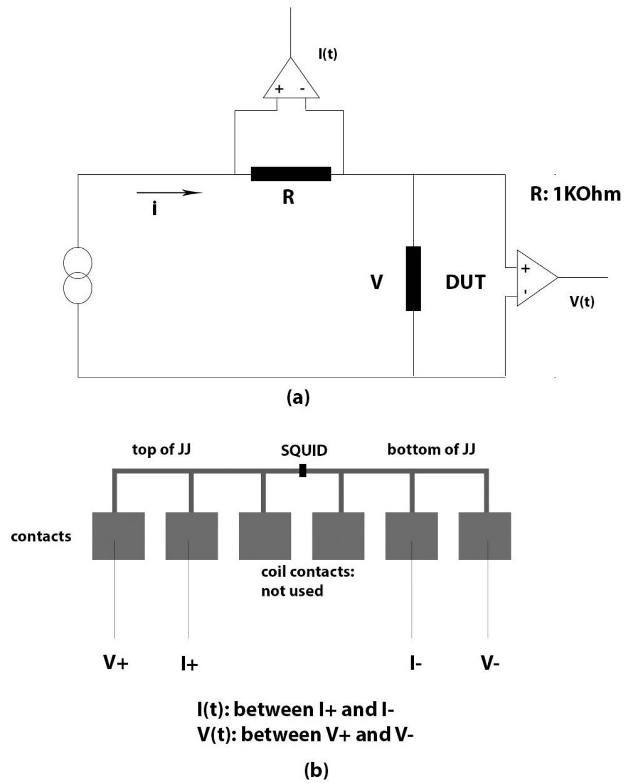

Figure 5.2: Bath cryostat measurement illustration: Obtaining an $I - V$ relation.

(a): Current source is used to send current signal across the device under test (DUT). Measuring the voltage across resistor of known value provides the means of recording this signal. After accounting for the resistor and the amplification, $I(t)$ is obtained. The current is set to be triangular wave, oscillating around provided limits. Second set of device connections are used to measure the voltage across the DUT. $V(t)$ is obtained by measuring the voltage across the sample and accounting for the amplification; (b): Connection set-up for SQUIDs. There are two contacts connected to the bottom of the junctions (JJ) and two to the top. In case of measuring small junctions samples, the situation is analogous, even though the connections are spatially arranged differently.

$I - V$ characteristics were obtained with and without application of magnetic field. Because of the observed inhomogeneity in the height of the wafers, the decision was taken not to use the fabricated SQUID coils, but instead to use external coil as magnetic field source. This is also identified on figure 5.2. In that way we made sure that potential shorts between the coil and the devices will be avoided.

To control the current and respectively the field the external coil was producing, second current source was used. It was operated, as all other instrumentation by a LabView vi. Entries 14-17 from Appendix D provide full history of the measurements and calibrations performed with the instrumentation. Links are provided to the raw, plotted data, where the programs and algorithms used are also enclosed.

Small samples

The small samples of Josephson junctions were measured, as well as structures from the three successful wafers. Unfortunately all of the junctions showed resistor behaviour in the $10K\Omega$ range or random signals, demonstrating that the junctions were most probably provided too high currents and due to that destroyed. The possibility exists that the junctions were sealed by the insulation layer, as their surface area is very small, making a bad connection to the measurement pads. For the SQUIDs this is not an issue, as the connections are not laid from the junctions themselves. Entry 5.(A, B) from Appendix D provides the records from the wiring and measurements.

Wafers

Several tens of SQUIDs from different parts of the successful wafers were measured. Entries 14-17 from Appendix D present the process of the sample preparation, measurement and general outcomes. In the majority of the cases we measured shorting or floating signals which suggests that the devices had connection issues or other defects in the bulk. Several measurements also yielded structures with very high critical current (above mA), going out of the range of the machinery. These cases are all discussed in the analysis section. However, due to the volume of the measurement data, here only the successful measurements are presented. All of the successful devices were from wafer 8. To avoid ambiguity, the parameters of those devices are identified below.

Device	Junctions	Resistors width	Washer area
W8S1	3x3 μm	$3\mu m$	$182\mu m^2$
W8S2	3x3 μm	$3\mu m$	$256\mu m^2$
W8S3	3x3 μm	$2\mu m$	$256\mu m^2$

Table 5.1: Properties of the successfully measured devices.

** The parameters are given according to the intended values in the design. For the washer the inner area is given. Resistor length and thickness are fixed in the design ($12\mu m$ and $75nm$ respectively). The devices naming W8S1-3 is only for simplicity and stands for wafer 8 SQUID 1-3.

These structures were on one of the pieces cut from wafer 8. The location of the devices is identified on figure 5.3 (on page 27).

On the SQUIDs two types of measurements were performed: single $I - V$ characteristics and sweep measurements (sweeps). The sweeps were performed in the following way: The voltage sent to the coil-controlling current source was varied between 0 and some end value (different throughout the measurements) in particular amount of steps. This resulted in a variation of the coil current and respectively the field it produced. At each step an $I - V$ characteristic was taken. Every current-voltage relation in the experiments consisted of 5000 sample points, enclosing several periods of the triangle current wave, used as current signal across the samples. This means that every $I - V$ in fact consisted of several superimposed characteristics. In that manner the measurements were more reliable and precise. Both the single and sweep measurements can be used to obtain the critical current of the devices. From the sweeps, critical current modulations with respect to the applied field were also extracted. Following are the obtained plots with major remarks on the relevant measurement details. For deep discussion and evaluation of those results, the reader can address the Analysis chapter.

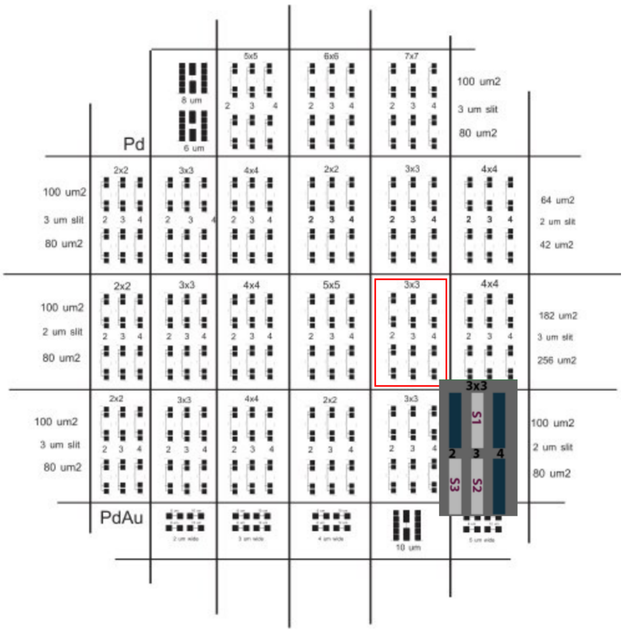

Figure 5.3: Successfully measured devices from wafer 8.

The location is given on the schematic of the wafer. S1-3 stands for SQUID 1-3.

I-V characteristics

Here only a selection of the $I - V$ characteristics is shown, demonstrating the highest current range measurements, and respectively showing in greatest detail the devices behaviour– figure 5.4 and figure 5.6 (on page 28). Appendix F provides all the plots obtained. They all look similar, but particular differences can be identified. This is most likely due to random variables entitled to the process, or due to the fact that the devices were changed in the process of measurement. Changes are subtle but even such small variations can later influence the performance of the sensors in their final task.

For the last device (W8S3) we obtained a slope, superimposed over the characteristic. This was due to the fact that one of the connections of the cryostat was broken. Therefore, one of the contacts from figure 5.2 (b) (on page 25) was not functional (V-). This forced us to perform 3-terminal sensing instead of 4-terminal and use one connection as both I- and V- terminal. Due to that the internal resistance of this terminal was also observed. Figure 5.5 (on page 28) illustrates the issue. The characteristic of W8S3 therefore was extracted by subtracting a linear fit made in the range of voltages around $V = 0$.

From those plots and the ones in Appendix F a lot of information was extracted, which will become clear in the analysis. Critical currents were identified and the devices acted similar to (at least) Josephson junctions. The sweep measurements, explained in the following subsection were used to identify if SQUID behaviour is present, according to the expectations of figure 2.7 (on page 9). This was the crucial, as a measurement of critical current does not unambiguously suggest that a device is a SQUID. It is also possible that we measured single working junctions.

The list below summarizes the observations on the obtained plots which will be further analyzed:

1. Critical current can be observed (derived) from all current-voltage relations
2. The critical current is different when comparing the first two devices (W8S1,2) and the third one (W8S3)
3. On the $I-V$s in this section and the ones in Appendix F hysteresis and multiple ”jumps” (transitions) of the current are visible (the characteristics are not smooth)
4. Some of the current-voltage relations show differences in repeated measurements

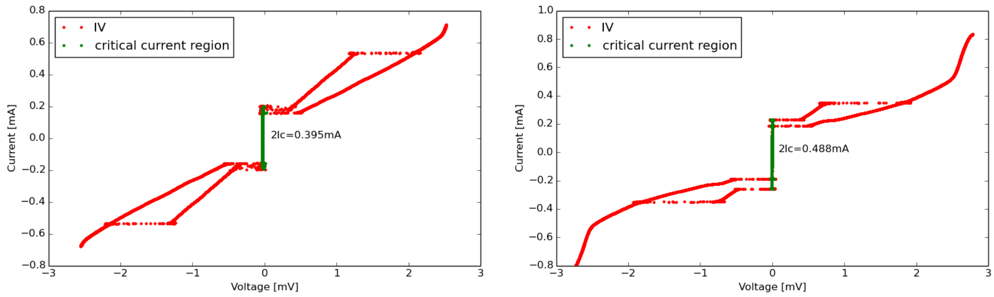

(a) (b)

Figure 5.4: $I - V$ plots.

Plots for the first two devices with $1mA$ range of the applied triangular wave current signal. (a) W8S1; (b) W8S2;
From the plots critical current can be identified (from vertical region of vanishing voltage in green). The approximate critical currents are also given (the reader can see $2I_c$).

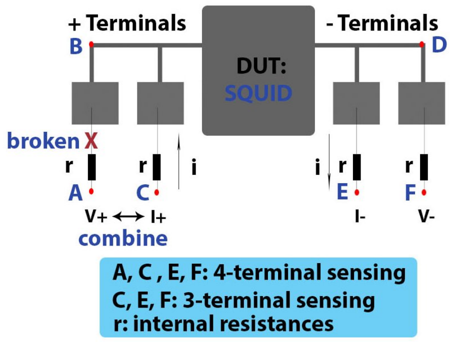

Figure 5.5: Comparison between 3– and 4– terminal sensing.

In the ideal case when all contacts are functional, current is sampled between points C and E and the voltage measured across points A and F which produce the same measurement as is the voltage is measured between points B and D. When one of the connections for sampling voltage is broken (A), we are forced to use the closest available contact (C) for the sampling. This imposes that the voltage is sampled across points C and D (analogous to C and F). This superimposes the voltage drop of the internal resistance (r) of connection C on top of the desired voltage drop of the DUT.

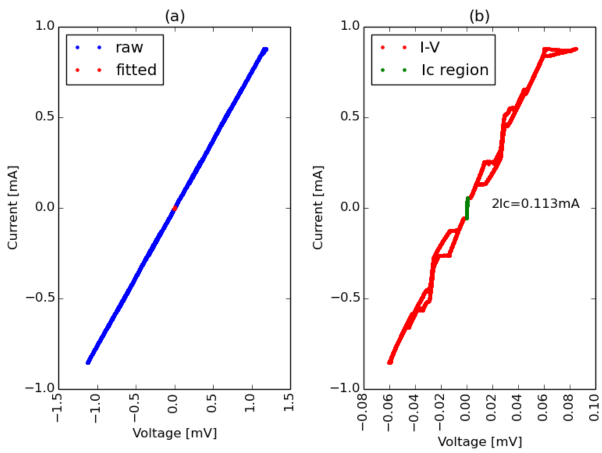

Figure 5.6: $I - V$ characteristic of W8S3 after slope extraction.

(a) Initial characteristic and fitted area; (b) Obtained characteristic after slope removal. Extracted slope corresponded to current-voltage relation of a 1.25Ω resistor; The range of the applied current is $1mA$. The reader can also find the identified critical current ($2I_c$).

Field modulation characteristics

Modulation characteristics were obtained from the magnetic field sweeps, explained earlier. As shown on the $I-V$ plots of the last subsection, twice the critical current was obtained at every step of the sweep. Later this critical current was plotted versus the magnetic field applied. Working with twice the critical current still unambiguously shows the behaviour of the devices. From the $I-V$s in the previous subsection it is already visible that there is no perfect symmetry, so it was not going to be accurate to search only for critical current in the positive range. Figures 5.7-5.9 (on pages 30-31) show the modulations obtained. [1] Table 5.2 (on page 31) show the approximate modulation depth in percentages.

Based on the design calculations, we expected to observe modulation for field change of several μT (in particular about $6\mu T$) (Appendix A). On figure 5.7 therefore the field steps were not arranged in manner to detect this modulation, but instead the measurements provided information on the devices characteristics in the wide-field (mT) range. On figure 5.8 the magnetic field could not be determined, as the coil which was used was displaced, not enclosing the samples in appropriate way. Therefore, the sample was not exposed to homogeneous magnetic field, but instead was at the edge of the coil, in the field fringing region (figure 5.10 (b), page 31). This implies that the magnetic field was a lot lower than intended. For those measurements, the field was still set-up in the mT range, but because of the reasons just explained, it is known that the field through the SQUID loop was a lot lower. The two plots on this figure however still provide a lot of useful information and figure 5.8 (a) even shows similar to the expected shape of SQUID modulation in magnetic field (for W8S1). This measurement in particular was canceled due to error in the setting-up of the program (far too many sweep steps were defined). However, that is why in those initial steps of program execution the field was in even lower ranges, probably explaining why the modulation could be observed.

In some of the sweeps explained above (figures 5.7 (b, d, f) and 5.8 (b)) other type of modulation is observed. This result in particular raises the question of junction field modulation. When using external coil, no matter how close to the samples, it is still a lot further away, compared to the coils fabricated on the very top of the SQUIDs. Therefore we cannot neglect the parallel component of the magnetic field, crossing the Josephson junctions (figure 5.10 (a), page 31). Field modulation in separate junctions is also possible [20] and the main suspicion is that the wide-range modulation is exactly due to this. This problem is analyzed further in the report.

After re-evaluation of the set-up and new coil calibration, narrow-range magnetic field modulations were also performed. Unfortunately, for these measurements W8S1 and W8S3 were not functional anymore. Therefore, the intended sweeps could be performed only with W8S2. Figure 5.9 provides the obtained plots. Considering the amount of steps and the field ranges, the critical current could be determined almost for every $1-2\mu T$. The modulation depth is very small, and still the predicted in the design calculation period of oscillation is not observed. However, those plots were also considered in the overall analysis.

The list below summarizes the observations on the obtained plots which will be further analyzed:

1. SQUID-like modulation was observed in one of the measurements 5.8 (a)
2. Junction field modulation is suspected in some of the wide-range measurements 5.7 (b, d, f), 5.8 (b)
3. The modulation depth of all tests seem too low
4. The narrow-range tests show consistent oscillations, but there are no solid signs of the predicted modulation

[1] Negative fields on the figures result from the current-voltage characteristic of the modulation coil current source. It is addressed in Appendix D, entry 15.

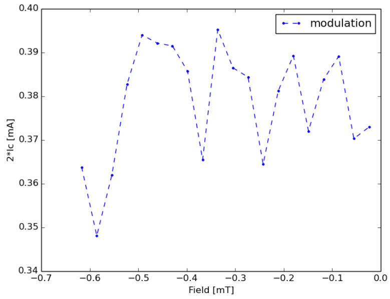

(a)

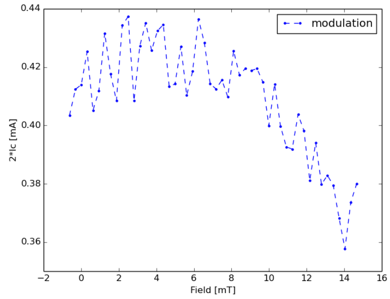

(b)

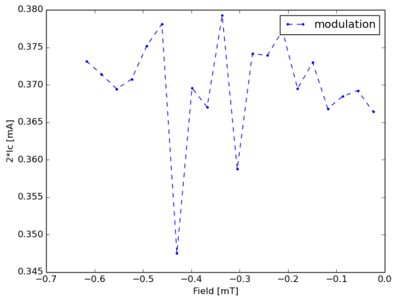

(c)

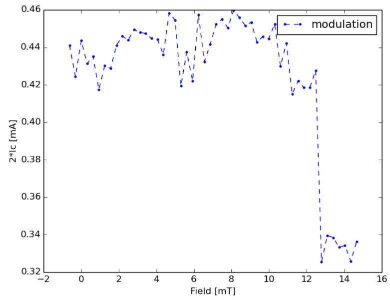

(d)

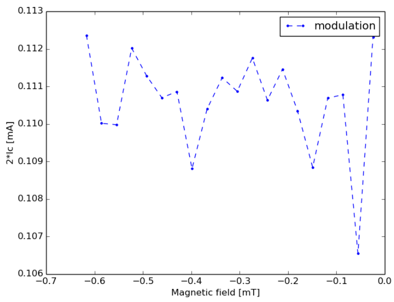

(e)

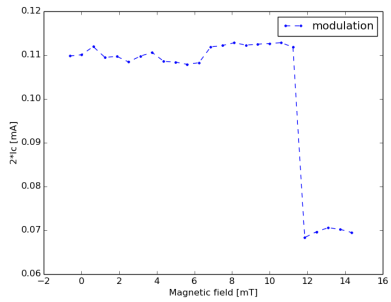

(f)

Figure 5.7: Critical current modulations obtained for W8S1-3 in wide-range magnetic field measurements.

(a) Modulation for $0.6mT$ magnetic field range in 20 steps, W8S1; (b) Modulation for $16mT$ magnetic field range in 50 steps, W8S1; (c) Modulation for $0.6mT$ magnetic field range in 20 steps, W8S2; (d) Modulation for $16mT$ magnetic field range in 50 steps, W8S2; (e) Modulation for $0.6mT$ magnetic field range in 20 steps, W8S3; (f) Modulation for $16mT$ magnetic field range in 25 steps, W8S3;

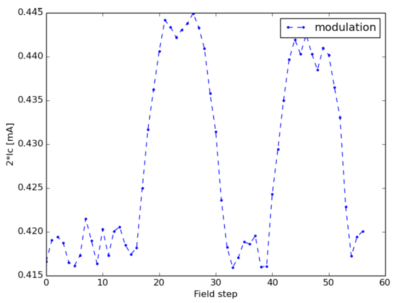

(a)

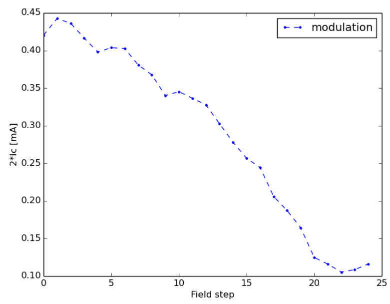

(b)

Figure 5.8: Critical current modulations obtained for W8S1 with unknown magnetic field values.

(a) Modulation for increasing unknown magnetic field in 57 steps, W8S1; (b) Modulation for increasing unknown magnetic field in 25 steps, W8S1; SQUID-type modulation is observed in (a). For this measurement the field is in the lowest ranges, as the program execution was canceled at early stage. The range for the other sub figure should be a lot higher, as then the program was fully executed.

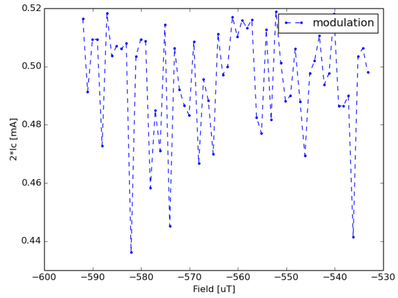

(a)

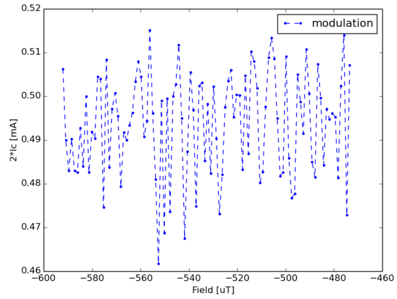

(b)

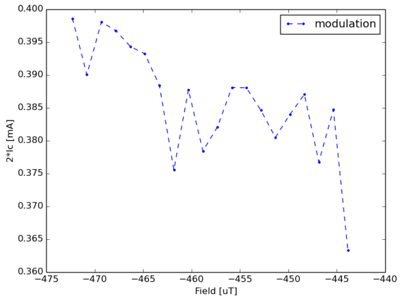

(c)

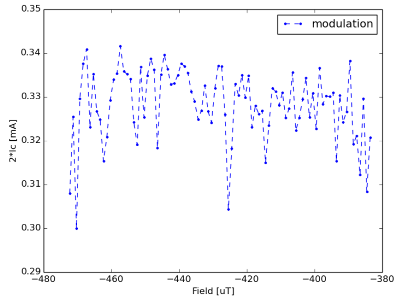

(d)

Figure 5.9: Critical current modulations obtained for W8S2 in narrow-range magnetic field measurements.

(a) Modulation for $60\mu T$ magnetic field range in 60 steps, W8S2; (b) Modulation for $120\mu T$ magnetic field range in 100 steps, W8S2; (c) Modulation for $30\mu T$ magnetic field range in 20 steps, W8S2; (d) Modulation for $90\mu T$ magnetic field range in 90 steps, W8S2;

Plot	**Modulation depth [%]**
Figure 5.7 (a)	12
(b)	19
(c)	9
(d)	30
Figure 5.8 (a)	7
(b)	78
(c)	6
(d)	40
Figure 5.9 (a)	16
(b)	10
(c)	9
(d)	12

Table 5.2: Approximate modulation depths obtained from the measurements.

Modulation depths are approximate and expressed in percentage. The numbering follows the figures in chronological order. The wide-field range tests yield the deepest modulations.

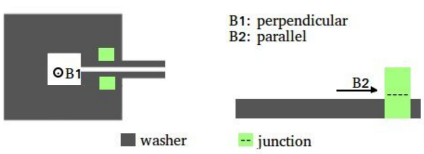

(a)

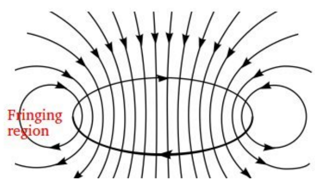

(b)

Figure 5.10: Magnetic field components.

(a) The components of the magnetic field mentioned in the text. The setting of the magnetic field refers to the perpendicular component. The parallel component cannot be easily derived; (b) Fringing circular coil region;

VI. Analysis

In this chapter the reader will find all analysis regarding the results, as well as discussion on the problem of a SQUID integration in a TI device.

VI.I Measurement outcomes

The analysis follows the summarized observations in the Results chapter, including the additional investigation performed.

I-V characteristics

On all current-voltage relations presented in the previous chapter and in Appendix F, a clear transition was observed. Leaving out for now the discussion of hysteresis and the other transitions (voltage "jumps") on the plots, it should be noted that being able to measure critical current is already a step of great value for the research. This gives solid proof that there are functional junctions on the devices. From the $I-V$s it cannot be unambiguously identified if the measured device is a SQUID or a single junction. When taking in consideration the intended junction size on the measured devices (3x3 μm which gives $\approx S = 10^{-8} cm^2$), and the oxidation conditions used for their fabrication (P_{O_2} of $0.1 mbar$), we can address figure B.1 from Appendix B (on page 45). According to it, if we take an approximated critical current density (J_c) of $1000 A/cm^2$ for pressure $0.1 mbar$ (being in the region of one of the obtained in the past calibrations– in blue), then the critical current of a junction should be in the range of $0.1 mA$ ($I_c = SJ_c$)– twice the critical current in the range of $0.2 mA$. This order of magnitude agrees with the values of the observed critical currents on figures 5.4 and 5.6 (on page 28). However, the result has to be taken with caution. Due to the fact that the successfully measured devices were from the same wafer, a new oxidation curve could not be prepared. The junctions effective size is also a variable, as in every fabrication step the manipulations performed on the wafers can influence the structures. We are therefore allowed to work only with approximations and in the single $I-V$ case it cannot be evaluated, based on the old calibrations, if the measured devices are SQUIDs or just single junctions. From the current-voltage relations it is clear that the third device (W8S3) has a lower critical current than the rest of the measured devices. This gave two possibilities- either W8S1 and W8S2 were functional SQUIDs and W8S3 a single junction, or the critical current was varying too rapidly across the wafer. This is not impossible, as the oxidation pressure for this wafer was very low and there was a chance that the tunnel barrier is very thin and inhomogeneously distributed from device to device. Therefore, the modulation characteristics of the devices were the only unambiguous way of identifying a device as a SQUID or not.

Further, the focus is brought to the hysteresis observed on the plots. Regardless all initial preparations and calculations, we still observe it. It is possible that the very high critical current is again the reason. Another possibility is that the shunt resistance is too big. Here a curious result is applied to assist the discussion. From three of the sweeps on which we observed solid critical current drop (figures 5.7 (d, f) and 5.8 (b), page 30), the $I-V$s of the first step was taken and compared to $I-V$ from the last steps. This is presented on figure 6.1 (on page 33). It is clear that the hysteresis is improved a lot. This provides the means of justifying that the critical current was most certainly the reason for the bi-stability. Therefore, regardless of the reasons for obtaining those critical currents (imperfections in the weak link or on general too low oxidation pressure), it is known that their value needs to be reduced for the future. In the very initial calculations in this report critical current in the μA range was predicted as suitable (Appendix C). Therefore, actions need to be taken towards achieving this. Deeper investigation of the oxidation calibrations is therefore needed and this is accounted for in the future recommendations.

The next observation on the $I-V$ characteristics are the extra voltage transitions at constant current.

Additional research was performed on this topic to identify that such characteristic leaps can be due to two possible reasons. The stacking of multi-layer tunnel barriers can happen after oxidation at the connection interfaces of the junctions, leading to formation of secondary weak links. Additionally, as Nb is type II superconductor, movement of potentially trapped in the Nb magnetic flux vortices can produce additional voltage disturbances.[25]

In the first case, it is possible that before laying the top Nb the junctions cap area to already have been oxidized, altering the junctions from the intended SNINS type to SNINIS (the interface between 1 and 5 on figure 4.1 (c), page 22). This provides reasoning why not only one transition would appear in the $I-V$ relation. Even though protection capping Al layer was provided, it had to be removed before the layering of the top electrode, therefore in the period of wafer transportation the oxidation most certainly happened. However, if that was the case, the $I-V$ would look a lot more symmetric.[40] Considering the second option, vortices might have been trapped in the Nb during the cool-down, and because the superconducting state is true energy balance state, preserved in the superconductor.[25] Those vortices can interact with the currents and move in the superconducting materials. This movement causes additional voltage drop and affects the critical current of the device. Vortices get easily trapped (pinned) in defected areas, around pinholes and edges and similar structures, as the current passing through the superconductor acts on them with a Lorenz force. Therefore, pinholes and other defects in the system make it more susceptible to this phenomena.[41] The unpredictable movement of vortices can also explain why the $I-V$s do not exactly the same when the measurements is preformed again later. To stay objective and enclose all possibilities, we established that the effects are most certainly due to the both processes combined.

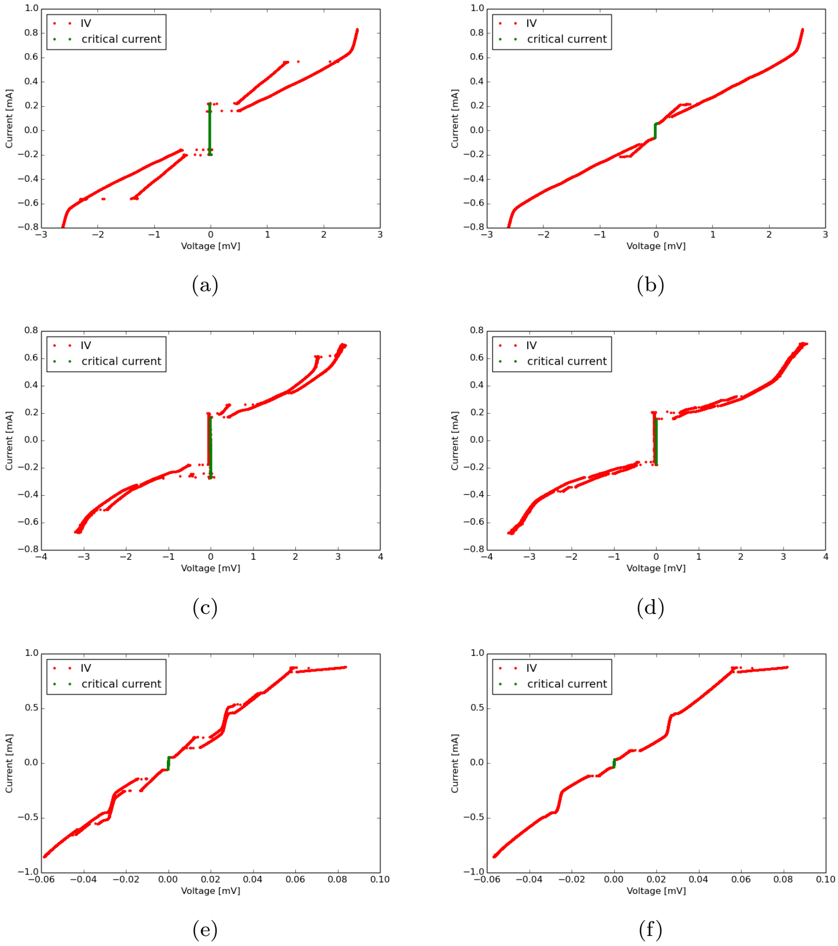

(a) (b)

(c) (d)

(e) (f)

Figure 6.1: Observation of vanishing hysteresis.

Some of the first and last $I-V$ plots obtained on the modulation characteristic measurements. (a) W8S1, first plot obtained in the measurement presented on figure 5.8(b); (b) W8S1, one of the last plots obtained in the measurement presented on figure 5.8(b); (c) W8S2, first plot obtained in the measurement presented on figure 5.7(d); (d) W8S2, one of the last plots obtained in the measurement presented on figure 5.7(d); (e) W8S3, first plot obtained in the measurement presented on figure 5.7(f); (f) W8S3, one of the last plots obtained in the measurement presented on figure 5.7(f); In those modulation measurements we saw solid critical current drop. It is therefore the reason for the hysteresis to lower.

Modulation characteristics

The most intuitive way to discuss the results of the modulation tests is to first search for signs of the expected rectified sinusoidal modulation, shown on figure 2.7 (on page 9). Similar picture we observed for W8S1 on figure 5.8 (a) (on page 30). It is unfortunate that for this measurement we do not know the exact magnetic field magnitude, but we can safely expect that it is in the μT range. The measurement was canceled at the initial stage of the program execution which was set in the range of $15mT$ for (at least) 1000 points, from which we executed only the first 57. This amounts to $\approx 15\mu T$ per step. Also, due to the fact that the samples were not exactly on top of the coil, but instead in its field fringing region due to set-up error, then this reduces the field even more. Based on the current discussion, it is safe to confirm that this device shows a SQUID behaviour. the modulation depth however shows to be very low (only 7%– from table 5.2, page 31). Therefore, the β_l parameter of this device is too high. Similar to the hysteresis issue, this might be due to the high critical current through the junctions, as β_l is directly proportional to it. This result once again makes a statement that full new oxidation calibration needs to be performed to show the most suitable region for the devices. The inductance of the system cannot be the major reason for the small modulation depth, as it strongly depends on the designed geometry. Of course, it is possible the dimensions to change in the fabrication process, but this cannot be responsible for the full effect. Recommendations on the improvement of the situation are stated further in the report. But unfortunately, it was not possible to make further measurements on W8S1. Attempts later identified that the device is no longer functional. This might be due to broken wiring or in the process of transportation and storage the device was damaged. There is a lot of insulation layer on the wafers, which causes charge build-up. It is not impossible that static electricity destroyed the device.

Other useful observations we obtain from the wide-range field tests (and the unknown field tests). On figures 5.7(b, d, f) and 5.8(b) (on page 30) we identified modulation, for which we suspected it is due to the parallel component of the field, crossing the junctions. Modulation with respect to magnetic field in Josephson junctions is observed as a sinc function (Fraunhofer) pattern.[20] Figure 6.2 (on page 35) illustrates the pattern. The first assumption was that this is the type of modulation we observe, more specifically only the first period of it. It is not possible to make a precise calculation as the parallel field of the coil, which crosses the junctions stack cannot be recorded. However, knowing that 1 flux quantum is of the order of $10^{-15}Wb(\Phi_0 = 2.067 \times 10^{-15}Wb)$, then taking the junction area (width: $3\mu m$, height: assuming the oxidation layer is at least $1nm$) as $\approx 10^{-15}m^2$, we know that the parallel field component needs to be about $1T$. This is of course impossible, as the parallel component is expected to be a lot smaller than the perpendicular component of the field (the one that we set, which was maximum in the μT range in our tests). Therefore, it is not possible to explain the plots with the Fraunhofer pattern. Possible explanation therefore for the observation of these is that the critical current might get suppressed due to complex interaction with vortices at that stage. Vortices can have very complex effect on the junctions behaviour, especially by means of suppressing the critical current. [42, 43]

As last, but not least, we discuss the narrow-range field measurement outcomes from figure 5.9 (on page 31. It is clear that the expected SQUID modulation is not present. There are oscillations about every several μT but those oscillations are not reassuring enough. The modulation depth, similar to the previous discussion is low and no specific patterns can be identified. This experiment forces us to conclude that W8S2 is not a SQUID device or there are other reasons due to which the modulation is suppressed. The presence of vortices is once again an option. Another possibility is that this device contained only a single functional Josephson junction at the first place. We considered as well that noise might be the reason, but the fact that no pattern was present at all easily disproved that. If the modulation is so subtle that the noise in the current measurement is bigger, then this modulation would not be on general relevant. As W8S1 and W8S3 were not functional anymore, further comparisons and measurements could not be done.

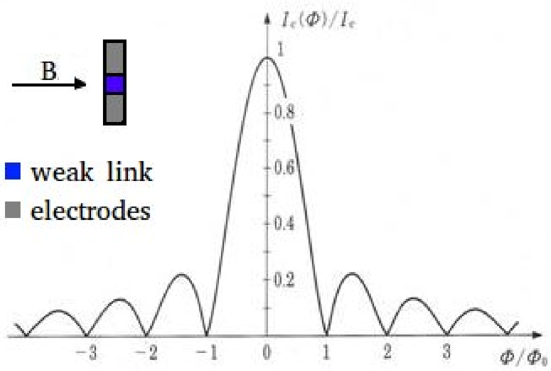

Figure 6.2: Magnetic field flux modulation in a single Josephson junction.

The modulation is periodic with a period of flux quantum. The modulation in the critical current (critical current, divided by the maximal critical current) is plotted versus the magnetic field flux(normalized with respect to the flux quantum). Here we consider the field crossing the junction stack. This field is identified with B_2 on figure 5.10. Adapted from [20].

Additional observations and summary

The fact that out of several tens of measured SQUIDs (above 30) only few showed junction or SQUID-like behaviour already implies that a lot of improvements are needed in the design. From most of the rest measurements we obtained $I-V$s of very high critical current, going out of the range for the instrumentation set-up. This directly identifies that we are measuring shorting between the Nb films, as the critical current of Nb only is a lot higher. Several low resistance curves (10Ω range) were also measured. This is most likely due to the fact that the junctions were destroyed by static electricity. Open leads were also identified, as well as many of the wire bonds made were easily detached. This implies that the surface of the electrodes (oxidized Nb) is not good material to lay connections on. The inhomogeneous height distribution which was already identified earlier in the report is most certainly responsible for many of the issues. With every procedural step the height error amplifies and this could lead to cross-linking of layers which should stay insulated. It is possible the top Nb to link to the lower layers and the current might flow through unpredictable pathways. Wrong insulation height also means that the junctions will not be defined in the intended way. All these might be the reasons for the low success rates observed, and also can explain why the devices show unstable behaviour (being functional for a particular period of time and destroyed easily).

To sum up, the analyzed measurements provided us with the needed information to draw conclusions for the design method which was deployed. The performed measurements also gave clues on which parameters need adjustment. The fact that with the many procedural flaws junction and even SQUID behaviour was present already proposes that the design and its methods are suitable. However, many adjustments need to be performed in order to deliver a suitable SQUID for the purpose of monopole detection.

VI.II SQUID integration in a TI device

To analyze the SQUID integrability in a TI device, it is needed to review the basic structure of such a device. Even though it is also still under design, the concept of its architecture is known.[5, 44] Figure 6.3 below provides overview of the TI device architecture and SQUID integration and will be discussed in the following evaluation. [1]

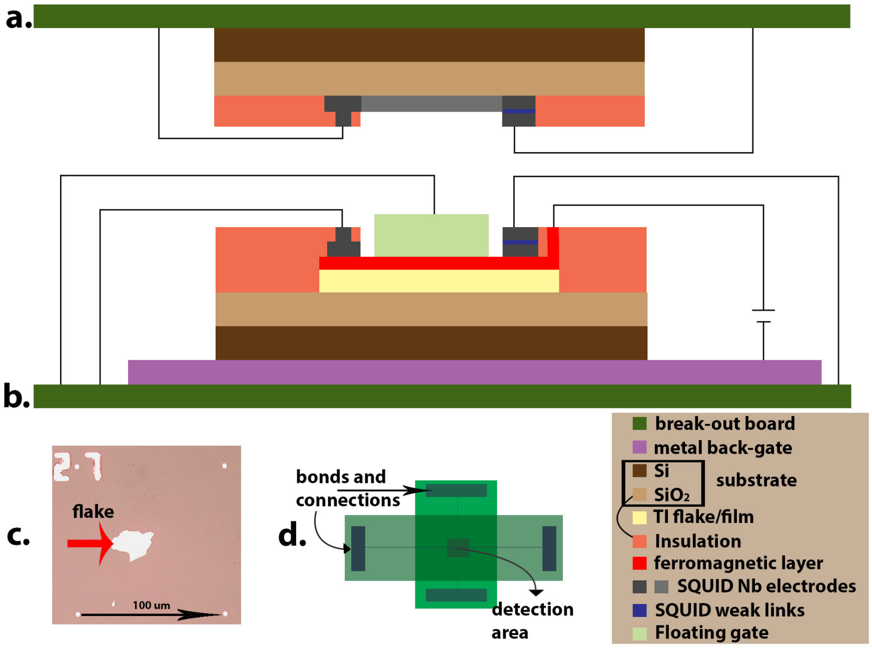

Figure 6.3: Integration of a SQUID in a TI device.

Overview of the TI device architecture can be found in (b), excluding the SQUID part of the diagram: A TI sample is positioned on a Si/SiO_2 substrate. The TI sample is back-gated with the help of metallic back-gate below and ferromagnetic layer on top, which both have a function to tune the TI properties (Fermi level and opening of the Dirac cone)**.[5] A floating gate is present on top of the TI sample to tune the charge impurities density that will have the function to induce magnetic monopoles. A SQUID can be positioned on the same substrate and fabricated on top of the TI sample; A SQUID can be also flipped on top of the sample but fabricated separately (a); The provided color legend refers to (a) and (b), which present a side view on the sample and SQUID. On the diagrams also the connections needed are provided: gating and top/bottom Nb SQUID connections. Controllable or measurable signals should be channeled to a break-out board. (c): Currently TI samples are obtained from TI crystals and transported on top of a substrate in the form of "flakes"– example of a flake; (d): Idea of how to keep the connections of the SQUID and TI sample away from the detection area when the flipping of (a) is used for the SQUID integration;

** Not part of the current research.

Looking at the architecture (figure 6.3(b), excluding the SQUID part), there are two options for the simultaneous application of the SQUID and TI part of the final device. They could be either separate components, or residing on the same substrate. The goal of this analysis is to review these two options and extract the limitations and ideas for their execution.

There are two methods currently being tested for the growth of the topological insulator– it can be deposited as a flake (figure 6.3 (c)) or if tests show to be successful– as a film.[44]. The limitations therefore follow– flakes are having irregular geometry and size, and normally the method currently used at the ICE group (obtaining the flakes from a crystal by exfoliation and transferring them on a substrate) distributes the flakes at random locations on the substrate. Research on the transportation is also being performed, but there are no summarized results available.[45] Opposed to the flakes idea is the deposition of TI film which can be patterned at the right sizes, shapes and locations. As in general the deposition of TI is still being tested, both the deposition methods will be included in the following discussion.

Considering that the TI film deposition and/or flake controllable transportation are successful, then the

[1]Once again the reader is asked to follow the color code carefully, as now different layers are in discussion and the detailing is not the same level as the device figures shown earlier.

TI samples would be at known locations on a substrate. Then SQUID masks, similar to the ones used now can be adapted and SQUIDs fabricated directly on top. This process will be most efficient, as then many SQUID-TI structures can be fabricated at once (figure 6.3 (b)), similar to the wafer processing of this research. However, as for measurements, samples need to be anyway cut down into pieces to fit on a break-out board, then the idea of "flipping" a SQUID on top of a TI sample is also applicable, and somewhat preferable at the initial stages when many TI device parameters will need adjusting. Fabricating SQUIDs and TI samples separately might enease the error handling per sample, but it will still be harder to position the SQUID at desired location on top of the measurand. Research on that is also currently performed in the ICE group [45], but in my analysis I propose several ideas. The main complication of the flipping technique will be the wiring that both samples will separately need. To this issue I propose the idea of figure 6.3 (d)– the two separate samples to be fabricated on non-symmetric substrates and the contacts kept away from the detection area, so wire bonding can be performed without the risk of damaging the samples. With this method the bonds can be laid high enough, while the samples can still be kept as close to each other as needed. To have control over the location of a SQUID, transparent substrates can be used and as for the fixation of the SQUID, additional insulation can be deposited around the TI sample (as a stand for the SQUID) to make sure that the SQUID can be successfully laid on top and at known height. This also inspires another mode of measurement. In the concept of this research the measurement idea was to vary the amount of charge impurities on top of a TI and measure the magnetic field variations. When varying the height of a SQUID on top of a TI sample, one can actually check for the magnetic field dependence with respect to height and derive if the expected monopole term ($\frac{1}{r^2}$) from the multipole expansion is present.

As the reader can already see, in both methods of arranging a TI device there are many unknowns, limitations, but also various techniques can be adapted to overcome those limitations. To summarize, fabrication of the device on single substrate will require the results of the TI deposition tests. If there are established procedures on depositing TI film or flake at precise location, then simultaneous fabrication will be possible and many TI devices could be produced as a single-piece devices. If those tests are not successful, then the TI and SQUID parts will have to be fabricated separately. Both methods have their advantages and disadvantages. While the singe substrate devices would be a lot more easy to transport to the side of measurement, their fabrication might take longer time and error handling (as SQUID and TI samples cannot be prepared in parallel). Opposed to that will be the separate substrate devices, for which the fabrication can be a lot faster and easier to troubleshoot, but then the positioning of the SQUID would require a lot of efforts and the transport of the device will always hide the risk of displacement. In both cases, the results of the ongoing researches in the ICE group should become available.

VII. Conclusion and Recommendations

VII.I Conclusion and Discussion

The research described in this report aimed to answer the following research question: *"What is a suitable way to design a SQUID that would be able to detect the predicted magnetic monopoles in topological insulators (mimicked by an applied external magnetic field)? What would be the further considerations in the application of a SQUID in a topological insulator device?"* The sub-problems of the research are listed and individually discussed below.

1. Is the design of such SQUID possible and why yes/not?

The design of such device is possible. Example design was developed and deployed and after its execution the further corrections needed were identified. The currently adapted methods yielded successful Josephson junctions. It was not possible to measure all devices, but SQUID-like modulation was also identified in the results. If the realization of a Josephson junction is possible, there is no limit to the goal of a SQUID design.

2. What were the adapted methods and was it possible to fabricate SQUIDs?
(From the fabricated SQUIDs which ones are promising solutions and which ones not and why?)

In the current research standard lithography and sputtering methods were used to layer vertical stacked Josephson Nb/Al/AlO_x/Al/Nb SNINS junctions on a square washer SQUID geometry. Based on the experimental methods explained in this report, SQUIDs were successfully fabricated on silicon wafers. From the fabricated devices suitable candidate for magnetic monopole detection was not identified. However, only 10% of the devices were measured. Based on the success rate of the tests, a decision was taken not to continue forward and instead identify the possible improvements and review the re-design possibilities. From the measurements overview gathered it is known that procedural and design execution flaws are the main reasons for not obtaining working SQUIDs. There were no evidences for other factors which restrict the fabrication of such in the future.

3. Are there corrections or other solutions that can be adapted for better/possible designs in the future?

The possible techniques and design corrections are stated in the Recommendations section. There are numerous ways by which the process of fabrication and devices manipulation can be improved to potentially yield suitable devices.

4. What were the encountered limitations and what are they due to?

The limitations regarding the process of SQUID design and fabrication came mostly from the establishment, and execution of the procedures. Considerable amount of the research consisted of calibrating the process of etching for junction definition and this procedure influenced all further outcomes. The project also did not have enough capacity for deep investigation of the outcomes at every fabrication step. Mostly visual observations had to be used for evaluating the quality of the samples which prevented us from identifying problems at early stage. Only at the last of the fabrication steps we could observe that the samples suffer from inhomogeneities in height which was of course a major problem. Therefore, the options for measuring and learning from the data was limited. Mainly assumptions could be drawn, but with the help of those we were able to identify the re-design problems in which wider range of limiting factors could be considered.

5. What would have to be considered in a design to give possibility for the sensor to be implemented in a hypothetical topological insulator device?

This problem was discussed from different points of view, considering the other on-going researches in the ICE group. Many of the proposed changes and adjustments therefore depend on the outcome of those. Two possible cases were considered for the overall TI device. In one of them the SQUID was reviewed as a separate component. To this situation, the design needs to be changed in a way to only account for the spatial arrangement of the device on the substrate. In order to efficiently hang a SQUID on top of a TI sample, it is needed to lay longer contact paths and position the wiring connections away from the detection area. Possibly transparent substrates can be used for easier localization of the sample which has to be measured. In the second case, it was proposed that the SQUID and TI sample can be fabricated on common substrate. In this situation the main consideration standing is the localization of the TI samples which will influence the manner of SQUID fabrication. Alteration of the device spatial arrangement will be again needed to account for the specifics of the other part of the TI structure fabricated beneath the SQUID. In both cases there were no factors identified to propose the impossibility of applying a SQUID in a TI device. The limitations regarding this problem are defined in the other researches in the group, namely– how to transport/deposit topological insulator samples at known location and what technique to use in bringing a SQUID at a desired location on top of the samples.

VII.II Future recommendations

Design and execution

There are no observation or experimental data to propose that the initial design of the devices is not suitable. Limitations are more due to the procedures and the design execution. This subsection discusses an improved strategy of work and the following subsection focuses on the procedures themselves.

The processing of wafers is providing advantages but also there are particular disadvantages. While from the many SQUIDs on a wafer there is a kind of guarantee to have good samples, even the slightest inhomogeneities can affect the results on every next step. A small sample has less effective area over which the processes can vary, so in the future investigations when time will not be restricted, it is recommended to follow different approach. Efficiency can be left aside at the initial stages and first proof of working concept developed. After the desired junctions and SQUIDs are providing satisfactory outcomes on a small sample, only then optimization for wafer fabrication should be done. It is important to keep track of the height distribution using surface techniques as an AFM, but different from now, it is good to perform it after every step in which patterning is performed and the unexposed photoresist removed. AFM cannot be applied when there is too big step difference in the height. So after the deposition of top Nb (when the structures will become a lot higher than the insulation around), then for example scanning electron microscopy (SEM) can be used. Before fabricating SQUIDs it is wise to focus on single junctions. This restricts the attention to first identifying if the tunnel barriers are functional.

After developing satisfactory junctions it is important to investigate in depth the oxidation conditions effect on the critical current. Full calibration should be performed from which the desired critical current obtained. In the current measurements we observed hysteresis most certainly already due to the very high critical current. Therefore, it is already reasonable to focus on higher ranges of oxidation pressures ($0.1mbar$ oxygen pressure for 1h is already providing too high β_c parameter). Other approach could be to extend the oxidation timing. There is no investigation performed on that from before. It is possible that longer oxidations can produce less pinholes in the weak links, and effectively improving the critical current problem. Similar tests for the shunt resistors are also recommended. There are no reasons to change the currently employed masks (for the development period), so they can be directly involved in the tests proposed above. The rest stages of work stay straightforward– once the desired junction parameters are selected, SQUIDs can be fabricated using the identified process parameters. It is important to also account for reproducibility. If particular samples, processed in the same way show different outcomes, then the reasons for that should be seeked before producing wafers on which the variation surely will become uncontrollable.

In analyzing the current measurements it became clear that many junctions might have been damaged due to storage and transport related factors. It is therefore suitable after the application of the insulation layer (which provides the danger of static discharge) all the samples to be taken out of their boxes only at the presence of ionizer (boxes should also be discharge safe). The same holds during wiring and mounting for bath cryostat measurements. Wire bonding can additionally have invasive effect on the structures. Laying wires induces stress on the contacts and it is crucial the bonds to be made as fast as possible. This was almost impossible now and wires hardly sticked well on the samples. The suspicion is that the top Nb layer on the contacts oxidizes and this alters the surface in an unintended way. To improve this, additional thin layer of Al can be deposited on top of the contacts. The wire bonder also operates with Al, so it is very possible to have better contact.

The measurement set-up will also need improvement. Currently the experimental data could not be fully deployed in the analysis, as there were missing measurement means for the components of the applied magnetic field. Such should be provided and calibrated with sources of known field, possibly with separately fabricated coils, identical to the ones on top of the SQUIDs. The top Nb mask can be used for that. This needs serious attention, as measurement precision is crucial in the later attempts for monopole detection. Noise handling strategy is also needed. Currently such was not adapted, as the research was not in such advanced stage, but once SQUIDs are identified and precise measurements start for the future, it will be crucial to make use of the modulation coils fabricated on top of the SQUIDs. Tests can be performed to find suitable frequency for noise cancellation.

If further proofs become available on the presence of vortices in the systems, then new masks can be introduced with intentional defects introduction to control the sites of pinning, keeping them away from the measurement area. However, this is problem that can be investigated only after measurements, which sends it to even later future situations. To this respect the design parameters will most certainly change in a way that cannot be predicted now. But vortex pinning is possible if cores of normal metal are introduced in the Nb electrodes. Vortices will reside in those normal cores as this will be more energetically favorable (vortices should have normal metal core according to the theory and in this way no energy will be needed to destroy the superconductivity in those areas).[25]

Procedures

Starting from the main source of deviations in the procedures– the etching procedures, there are several points proposed that most certainly can improve the fabrication:

- Investigate separately the RIE process: Maybe changing the SF_6 supplies will give good effect
- Possibly reduce the need for wet etching for the removal of the $Al/AlO_x/Al$ layer, as wet etching is not a process that can be kept under control: Ar etching can be used for the full trilayer, as different from SF_6, it is not selective to Nb only. Therefore at the junction definition step there will be no need of OPD etching and it will be needed only during lithographies. SF_6 etch will be needed only at the next step when the top trilayer Nb needs to be removed at undesired places, but then the effective etching area will be a lot smaller and the process more controllable.
- Consider changing the subtractive phase of the fabrication with additive steps: Instead of depositing full trilayer and exposing under etch mask to pattern the structures, the mask can be inverted and the structures patterned by lift-off instead of etching and the metal deposited after the first lithography. Mask inversion can be even avoided if negative (reversed) photoresist is used.

The lithography procedure did not show as problematic, but nevertheless, not all sizes of Josephson junctions were nicely defined at the final structures. Therefore point of recommendation is to replace the UV exposure with electron beam lithography which will define the edges with a lot better resolution (up to several nm [46]). This is possible in the MESA+ facilities, so there is no entitled resource issue. Other proposed change relevant to the lithography is to exclude cleaning of samples at the ultrasonic bath. The strong vibrations can have negative effect on the structure stability. Pieces of the devices might break off or cracks and other defects appear. Leaving the samples for several hours in acetone is better solution, or at least reduce the force of ultrasonication.

In accordance with the suspicion that the fabricated devices contain a secondary Josephson junction at the interface with the top Nb, procedural solution is available. At the beginning of every new layer deposition at the Nordiko system, RF substrate etching was performed to clean the top layer of the sample. In case the junction Nb is oxidized before connecting to the top Nb electrode, then for this step the timing or power of the RF cleaning can be increased.

Appendices

Appendix A SQUID size calculations

A.1 Considerations and formulas

Calculations were performed assuming circular SQUID loop, but the area of the SQUID stays analogous. The procedure from [1] was adapted.

STEP 1:

First the statistical angle was calculated for vacuum and TI with dielectric permeability of $\epsilon_2 = 100$ and magnetic permeability of $\epsilon_1 = 1$. The polarization P_3 was taken to be $\frac{1}{2}$. The equations used were:

$$\varphi = \frac{2\alpha^2 P_3}{(\epsilon_1 + \epsilon_2)(\frac{1}{\mu_1} + \frac{1}{\mu_2}) + 4\alpha^2 P_3^2} \tag{A.1}$$

$$\alpha = \frac{e^2}{\hbar c}$$

$$P_3 = \frac{1}{2}$$

STEP 2:

Two charge (monopole) densities were taken: $n_1 = 10cm^{-2}$ and $n_2 = 11cm^{-2}$ ($15m^{-2}$ and $16m^{-2}$) as requested by the project leader, due to the objective that such densities will be used in the TI device.[2] The idea was to calculate the SQUID size such as particular part of the output voltage modulation (within one period) to correspond to the flux change when transiting between the densities.

Further, two sets of calculations were performed as the flux change to correspond to a whole period of Φ_0 and to $\frac{\Phi_0}{\pi}$. The second calculation was inspired by [3] which states the maximal linear region that can be achieved for the voltage output. It corresponds to flux change of $\frac{\Phi_0}{\pi}$ in a flux-locked loop circuit, in which a SQUID is fed back its screened flux. Thus, calculations were done for the 2 limiting cases.

STEP 3:

Knowing the densities, the magnetic flux change was derived the following way:

$$B_{monopoles(1)} = n_1 \varphi \tag{A.2}$$

$$B_{monopoles(2)} = n_2 \varphi \tag{A.3}$$

With:
B: the magnetic induction

STEP 4: From here:

$$\Delta\Phi_{monopoles} = \Delta B S. \tag{A.4}$$

$$S = \frac{\Delta\Phi_{monopoles}}{\Delta B} \tag{A.5}$$

By selecting $\Delta\Phi_{monopoles}$ to be $\frac{\Phi_0}{\pi}$ or Φ_0, it was possible to estimate the area and therefore the maximal radius, knowing for a circle $S = \pi r^2$.

Numerical results

To avoid mistakes the actual calculation was performed in Matlab. The reader is referred to the program in the next appendix section.

A.2 MATLAB program

The code, based on the calculation procedure is displayed below. To adjust to SI measurement unit system, the parameter α from equation 2.1(on page 3) was redefined as it was given in the article in CGS (centimeter-gram-second) system. The calculation of magnetic induction and flux were already re-adjusted to SI when explaining the procedure in the main text in equation 2.2 (on page 3). The new α coefficient is given as follows in SI:

$$\alpha = \frac{1}{4\pi\epsilon_0}\frac{e^2}{\hbar c} \tag{A.6}$$

```
e1= 1.0; %dielectric constant 1
e2= 100.0; %dielectric constant 2 TI
m1= 1.0; %magnetic permeability 1
m2= 1.0; %magnetic permeability 2
n1= (10^15); %density electrons 1 in electrons/square meter
n2= (10^16); %density electrons 2
e0= 8.8*(10^-12); %dielectric permitivity vaccum

%some more constants:
pi=3.14;
e= 1.6*(10^(-19)); %[C]
hbar= 1.05*(10^(-34)); %[Js]
h= 6.6*(10^(-34)); %[Js]
c= 3.0*(10^8.0); %[m/s]
F0= 2*10^(-15);  %[Wb]

%specific to the problem/ as taken and modified from the article to SI UNIT system:
alpha=(e*e)/(4*pi*e0*(hbar*c));
P3=0.5;
fi= (2*(alpha^2)*P3);
fi= fi/((e1+e2)*((1/m1)+(1/m2))+(alpha^2)); %the statistical angle
fq= hbar*pi/e; %the flux quantum
disp('B1 is in Tesla [T]:');
disp(n1*fi*fq);
disp('B2 is in Tesla [T]:');
disp(n2*fi*fq);


deltaB= (n2-n1)*fi*fq;

Area= (F0/pi)/deltaB; %From relation B.S=Flux and linear region of fi0/pi

R= sqrt(Area/pi);
disp('Maximum radius [m]:');
```

```
disp(R);
```

Output

The calculation of the program was executed for output region of $\frac{\Phi_0}{pi}$ and Φ_0 respectively and it is clear that to have the output of the sensor in one period of the voltage modulation then the maximal radius would be $10\mu m$. This is assuming TIs of the same order of physical properties (ϵ and μ):

- Output region $\frac{\Phi_0}{pi}$
  inductance B_1 [T]$= 5.52 \times 10^{-7}$
  inductance B_2 [T]$= 5.52 \times 10^{-6}$
  maximal radius $[m] \approx 6.4 \times 10^{-6}$
  maximal radius $[\mu m] \approx 6.4$
- Output region Φ_0
  inductance B_1 [T]$= 5.52 \times 10^{-7}$
  inductance B_2 [T]$= 5.52 \times 10^{-6}$
  maximal radius $[m] \approx 1.1 \times 10^{-5}$
  maximal radius $[\mu m] \approx 10$

```
>> Squid_01
B1 is in Tesla [T]:
   5.5152e-07

B2 is in Tesla [T]:
   5.5152e-06

Maximum radius [m]:
   6.3927e-06

>> Squid_01
B1 is in Tesla [T]:
   5.5152e-07

B2 is in Tesla [T]:
   5.5152e-06

Maximum radius [m]:
   1.1328e-05
```

Appendix B Critical current density recorded in Nb/AlO$_x$/Nb junctions

A figure from the unpublished fabrication records [4] was extracted and analyzed to justify the assumptions that several tens of micro amperes is reasonable critical current.

The figure is displayed below:

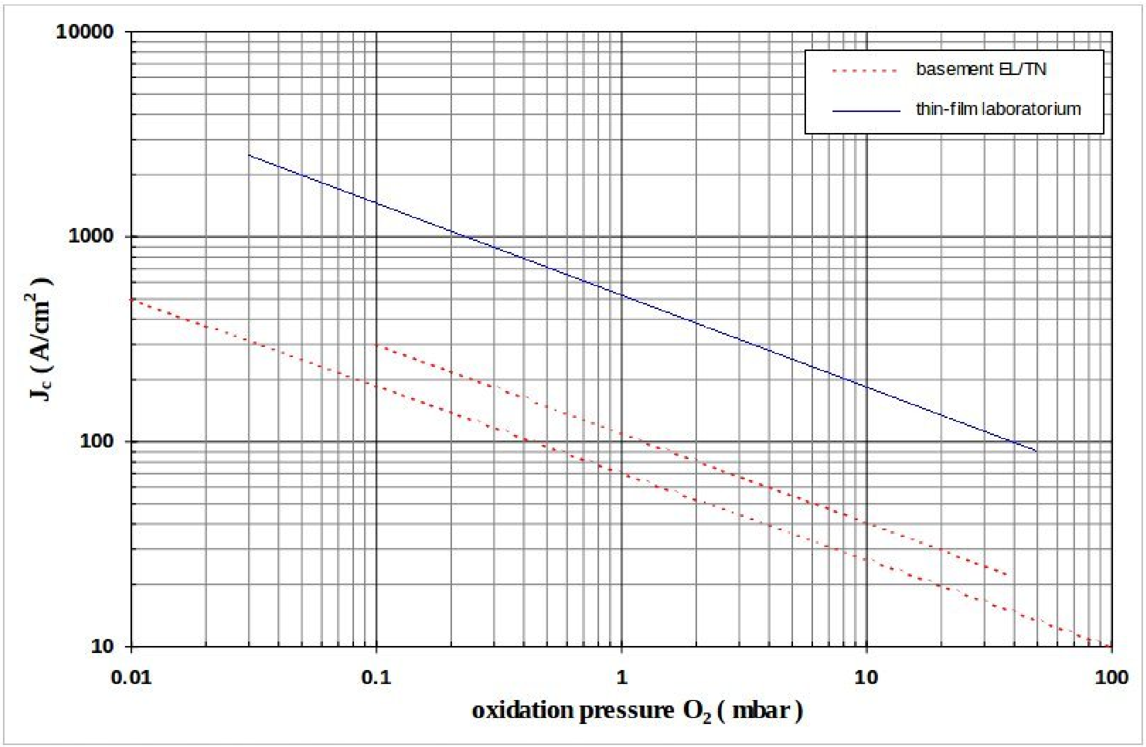

Fig 5: Critical current density as function of the oxidation-pressure.

Depending on the start conditions, especially the H_2O background-pressure in the loadlock, the oxidation curve can shift up or down. The two dashed lines are valued for the basement of the EL/TN building (our former lab), where the humidity was large. The upper curve is applied to the new thin-film-lab (April 1998), where the deposition rooms are conditioned and the humidity is lower than in the basement. It is not to be expected that this curve will shift a lot.

Figure B.1: Critical current density dependent on Al layer oxidation

Relation between critical junction current and oxidation pressure. Junction: Nb(150nm)/Al(5nm on which the oxidation is applied)/Al(5nm)/Nb(150nm). Adapted from [4]

From the figure one can derive plausible critical currents, as this diagram was experimentally derived. For several μm^2 junction area currents up to several tens of μA can be reached, using the simple relation that $I_c = J_c S$.

Appendix C Josephson junction example design calculation

This appendix provides example calculations on the design parameters for a Josephson junction, which can be then used to make a SQUID for further tests. The values were adapted from literature or the discussion in the first three chapters of the report.

Lets start from hypothetical desired value for β_l of 1, normally considered as appropriate in literature.[5, 6] If SQUID inductance of $20pH$ is chosen, inspired by table 3.2 (on page 17) from which only the most significant inductances are taken, the result for the critical current I_c will be derived, using equation 2.13.

$$I_c = \frac{\beta_l \Phi_0}{2L} \tag{C.1}$$

The numerical result after substituting is $50\mu A$. From Appendix B it is visible that such current is possible according to the previous testing in the university.[4] Performing oxidation testing can determine the right oxidation parameters to obtain such current in the current conditions. Substituting this result in β_c (equation 2.5 on page 8), it is received that for β_c below 1 (0.5 for example) and capacitance C of $0.6pF$ as calculated on page 15 (for junction area of $6\mu m^2$ and Al oxidized layer of $1nm$) the resistance R is having a value of 2.3Ω, which might be easily tuned by deposition of shunt resistor (metal layer of known thickness for example):

$$R = \sqrt{\frac{\Phi_0}{2\pi I_c C}} \tag{C.2}$$

Additionally, for the results here and temperature of $4K$ (bath cryostat), the Γ parameter will be only 0.003 (equation 3.3 on page 13).

In the experiments the condition for the inductance cannot be easily managed, as it will become clear only after the SQUID output is observed, but the results above show that junction of several μm characteristic size is reasonable value for this project. Imposing particular variation in the numerical results, it is good to design SQUIDs with varying sizes of the characteristic dimensions and the same for the junctions. The ranges are however known and the demonstration here should have assured the reader in that statement.

Appendix D Project log book

This appendix refers to the project log book. It is submitted in combination with the current report, to serve the following functions:

- Overview of tests and manipulations (Log book entries numbered in chronological order)
- Overview of all procedures used and their history of calibration (Procedures chapter)
- Overview of the machines and facilities used (Procedures chapter)

Appendix E Wafer structures examples

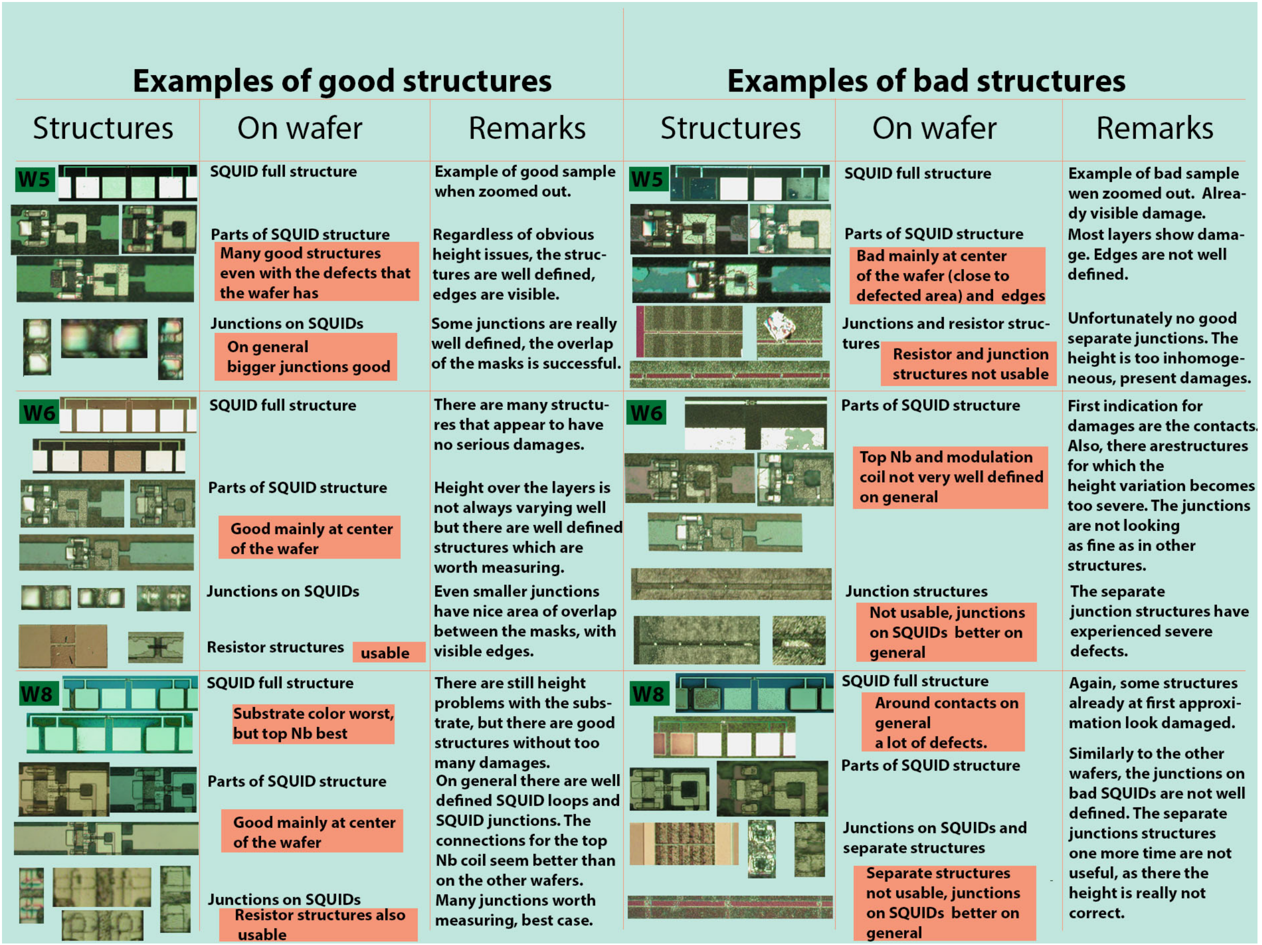

Figure E.1: Example structures

Examples of good and bad-looking structures with justification of the evaluation. Images of particular structures are presented, with reference to the wafer on which they reside.

Appendix F I-V characteristics

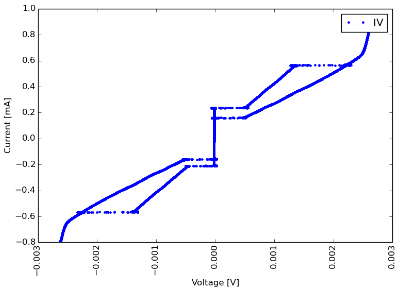

(a)

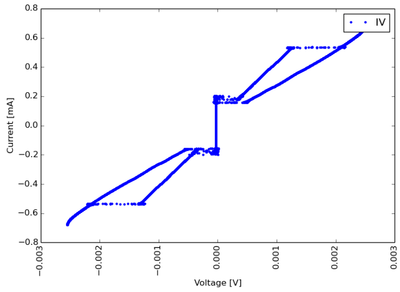

(b)

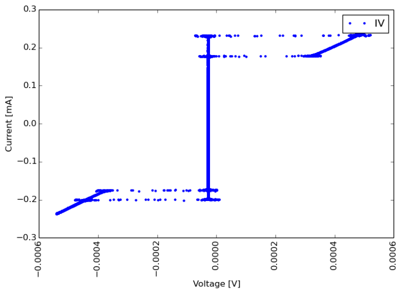

(c)

Figure F.1: All $I - V$ plots for W8S1.

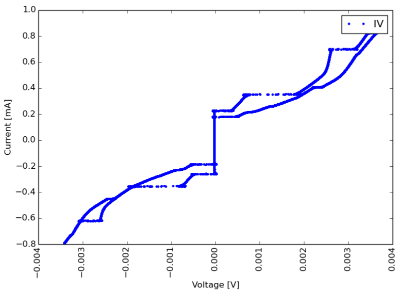

(a)

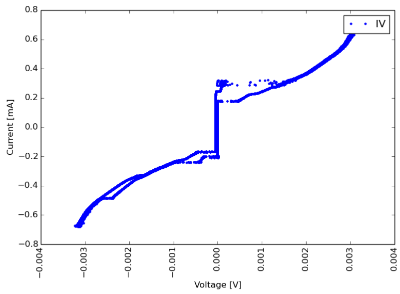

(b)

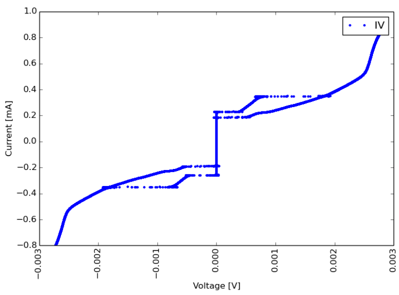

(c)

Figure F.2: All $I - V$ plots for W8S2.

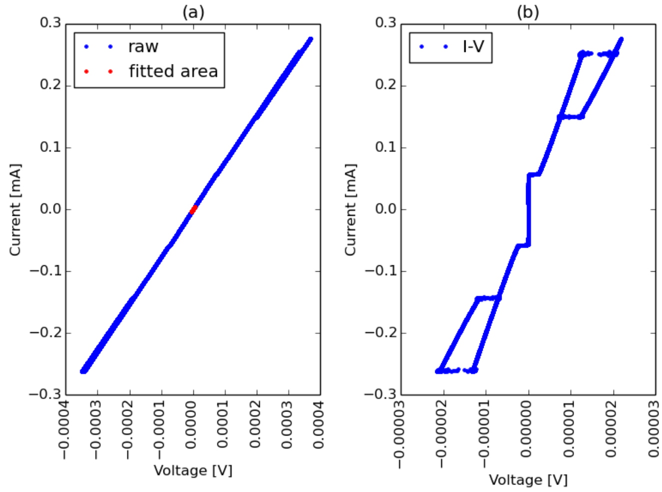

(A)

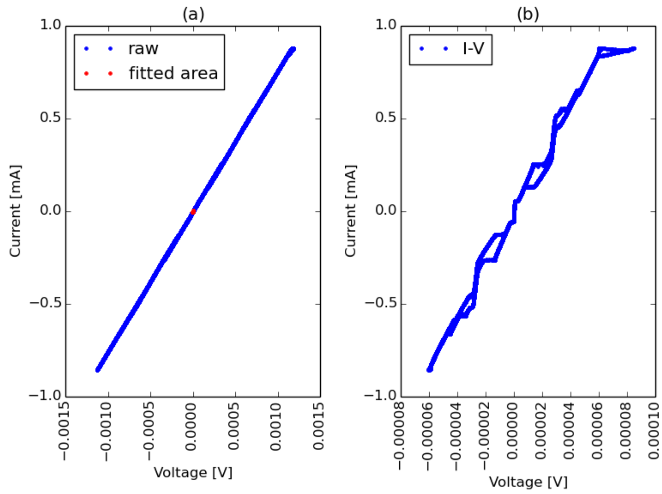

(B)

Figure F.3: All $I - V$ plots for W8S3.

(a) Raw characteristic; (b) Extracted characteristic after slope removal;

References

Citations from definitions

[1] M. Cyrot *et al.* *Introduction to superconductivity and high-Tc materials.* World Scientific Publishing, 1992, ISBN: 9810201435. **Chapter 1: Introduction**.

[2] M. Cyrot *et al.* *Introduction to superconductivity and high-Tc materials.* World Scientific Publishing, 1992, ISBN: 9810201435. **Chapter 6: Josephson effects**.

[3] Shun-Qing Shen. *Topological Insulators: Dirac Equation in Condensed Matters.* Springer Science and Business Media, 11 January 2013, ISBN: 978-3-642-32858-9. p.6.

[4] Science daily, January 29, 2014. [Online] Available from: `http://www.sciencedaily.com/releases/2014/01/140129164807.htm`, [Last Accessed: Sunday 21st June, 2015].

[5] E. Akhmedov. **Majorana neutrinos and other Majorana particles: Theory and experiment**. arXiv:1412.3320v1 [hep-ph], Cornell University library. 10 December 2014.

[6] F.A. Ferri *et al.* *Atomic Force Microscopy - Imaging, Measuring and Manipulating Surfaces at the Atomic Scale*, Edited by Victor Bellitto. InTech, 2012, ISBN: 978-953-51-0414-8. **Chapter 3: Magnetic Force Microscopy: Basic Principles and Applications**. p.39.

[7] Xiao-Liang Qi *et al.* **Inducing a magnetic monopole with topological surface state**. *Science*, 27 February 2009, **323** (5918): 1184-1187.

[8] Rundong Li. *Exotic particles in topological insulators* Phd thesis. Stanford University. July 2010. **Chapter 2: The image magnetic monopole**.

[9] J. Clarke *et al* (ed.). *The SQUID handbook.* Vol. 1: Fundamentals and technology of SQUIDs and SQUID systems. Wiley-VCH, 2004, ISBN: 3-527-40229-2. p.30.

[10] H. Ibach *et al.* *Solid-State Physics: An Introduction to Principles of Materials Science*, 4th edition. Springer, 2009, ISBN: 978-3-540-93803-3. p.303.

[11] H. J. W. Müller. *Introduction to Quantum mechanics: Schrödinger equation and path integral.* World Scientific Publishing, 2006, ISBN: 981-256-691-0. p.251.

[12] Sigma-aldrich. *Lithography Nanopatterning Tutorial Lithography Nanopatterning*, [no date]. [Online] Available from: `http://www.sigmaaldrich.com/materials-science/micro-and-nanoelectronics/lithography-nanopatterning/tutorial.html` [Last Accessed: Sunday 21st June, 2015].

[13] AJA International Inc. *What is sputtering?*, [no date]. [Online] Available from: `http://www.ajaint.com/whatis.htm` [Last Accessed: Sunday 21st June, 2015].

[14] MNX: MEMS and Nanotechnology Exchange. *Etching processes*, [no date]. [Online] Available from: `https://www.mems-exchange.org/MEMS/processes/etch.html` [Last Accessed: Sunday 21st June, 2015].

[15] Charles P. Poole Jr. *Encyclopedic dictionary of condensed matter physics*, 1st edition. Elsevier Inc., 2004, ISBN: 0-12-088398-8. p.2.

Citations from main text

[1] MESA+ Institute for nanotechnology. University of Twente. **Interfaces and correlated electrons**. *Research topics: Topological insulators*, [no date]. [Online] Available from: `http://www.utwente.nl/tnw/ice/research/topo/` [Last Accessed: Sunday 21st June, 2015].

[2] Topological insulator today, *topological insulator news and research papers*, last updated March 12 2015. [Online] Available from: `http://topologicalinsulator.net/` [Last Accessed: Sunday 21st June, 2015].

[3] Yoichi Ando. **Topological insulator materials**. arXiv:1304.5693v3 [cond-mat.mtrl-sci], 3 September 2013.

[4] Joel E. Moore. **The birth of topological insulators**. *Nature International weekly journal of science*, 11 March 2010, **464**, 194-198.

[5] Xiao-Liang Qi *et al.* **Inducing a magnetic monopole with topological surface state**. *Science*, 27 February 2009, **323** (5918): 1184-1187.

[6] Joel Moore. **Topological insulators: The next generation**. *Nature Physics.* **5**, 378-380 (2009).

[7] A. Rajantie *et al.* **Magnetic Monopoles in Field Theory and Cosmology**. arXiv:1204.3073v1 [hep-th], 13 April 2012.

[8] L. D. C. Jaubert *et al.* **Signature of magnetic monopole and Dirac string dynamics in spin ice**. *Nature Physics*, 15 March 2009, **5**, 258-261.

[9] S. T. Bramwell *et al.* **Measurement of the charge and current of magnetic monopoles in spin ice**. *Nature*, 15 October 2009, **461**, 956-959.

[10] S. Ladak *et al.* **Direct observation of magnetic monopole defects in an artificial spin-ice system**. *Nature Physics*, 11 April 2010.

[11] Xiao-Liang Qi *et al.* **Inducing a magnetic monopole with topological surface state: Supporting online material**. *Science*, 27 February 2009, **323** (5918): 1184-1187.

[12] L. Zeng *et al.* **Inducing magneto-electric response in topological insulator**. *Journal of Magnetism and Magnetic Materials*, February 2013, **328**, 26–30.

[13] Prof. Dr. Ir. A. Brinkman. Chair Quantum Transport in Matter research group. University of Twente. *Discussion on initial SQUID design calculations.* **Conversation**, 16 February 2015.

[14] H. Hilgenkamp. *High-Tc SQUID magnetometers.* Phd thesis. University of Twente. Enschede, 1995, ISBN: 90-9008057-0.

[15] D. Adelerhof. *Second generation dc SQUID magnetometers: (double) relaxation oscillation SQUIDs.* Phd thesis, University of Twente. Enschede, 1993, ISBN: 90-9006513-X.

[16] H. Hilgenkamp. *High-Tc SQUID magnetometers.* Phd thesis. University of Twente. Enschede, 1995, ISBN: 90-9008057-0. **Chapter 1: Introduction**.

[17] J. E. Lenz. *Proc. IEEE* **78**, 973 (1990).

[18] M. Sawicki *et al.* **Sensitive SQUID magnetometry for studying nanomagnetism**. *Semiconductor Science and Technology*, 8 April 2011, **26** (6).

[19] J. D. Jackson. *Classical Electrodynamics.* New York: Wiley, 1962, ISBN: 0 472 43131 1. **Chapter 2: Bouldary-value problems in electrostatics I**.

[20] M. Cyrot *et al. Introduction to superconductivity and high-Tc materials.* World Scientific Publishing, 1992, ISBN: 9810201435. **Chapter 6: Josephson effects**.

[21] Liu, Yi, Sellmyer, D.J., Shindo, DAISUKE (Eds.). *Handbook of Advanced Magnetic Materials*: Vol 1. Nanostructural Effects p.299.

[22] M. Cyrot *et al. Introduction to superconductivity and high-Tc materials.* World Scientific Publishing, 1992, ISBN: 9810201435. **Chapter 1: Introduction: Superconductivity and superconducting materials**.

[23] C. J. M. Verwijs. *Fractional flux quanta in high-Tc/low-Tc superconducting structures.* Phd thesis, University of Twente. Enschede, 2009, ISBN: 978-90-9024316-0. **Chapter 2: Superconducting loops containing Josephson junctions**.

[24] Clarke *et al* (ed). *The SQUID handbook.* Vol. 1: Fundamentals and technology of SQUIDs and SQUID systems. Wiley-VCH, 2004, ISBN: 3-527-40229-2. **Chapter 2: SQUID theory**.

[25] M. Cyrot *et al. Introduction to superconductivity and high-Tc materials.* World Scientific Publishing, 1992, ISBN: 9810201435. **Chapter 2: Characteristic properties**.

[26] J. Clarke *et al* (ed.). *The SQUID handbook.* Vol. 1: Fundamentals and technology of SQUIDs and SQUID systems. Wiley-VCH, 2004, ISBN: 3-527-40229-2. **Chapter 1: Introduction**.

[27] Ing. D. Veldhuis. Technical staff member ICE group. University of Twente. *SQUIDs and Josephson junctions fabrication and techniques.* **Conversation**, 9 February 2015.

[28] H. Hilgenkamp. *High-Tc SQUID magnetometers.* Phd thesis. University of Twente. Enschede, 1995, ISBN: 90-9008057-0. **Chapter 2: Josephson junctions and autonomous dc SQUIDs**.

[29] H. Weinstock(ed.). *SQUID Sensors: Fundamentals, Fabrication and Applications.* Springer, 1995, ISBN 978-94-010-6393-7. p.258.

[30] V.J. Waal. *Low noise SQUIDs.* Phd thesis. University of Delft, 1983, ISBN: 90-9008057-0. p.46.

[31] D. Adelerhof. *Second generation dc SQUID magnetometers: (double) relaxation oscillation SQUIDs.* Phd thesis, University of Twente. Enschede, 1993, ISBN: 90-9006513-X. **Chapter 2: Present dc SQUIDs**.

[32] Ceramic industry. *Material Properties Charts*, [no date]. [Online] Available from: `https://www.ceramicindustry.com/ext/resources/pdfs/2013-CCD-Material\-Charts.pdf` [Last Accessed: Sunday 21st June, 2015].

[33] Goodfellow Cambridge Ltd., *Metals, Alloys, Compounds, Ceramics, Polymers, Composites*, **Catalogue**, 1993/94. [Online] Citation from: `http://www-ferp.ucsd.edu/LIB/PROPS/PANOS/al2o3.html` [Last Accessed: Sunday 21st June, 2015].

[34] M. Gurvitch *et al.* **High quality refractory Josephson tunnel junctions utilizing thin aluminum layers**. *Appl. Phys. Lett.*, **42**, 472 (1983).

[35] B. W. Maxfield *et al.* **Superconducting Penetration Depth of Niobium**. *Phys. Rev.*, 30 August 1965, **139**, A1515.

[36] C. Brons. **Low-Tc fabrication process**. [Unpublished], April 1998, University of Twente. Available from: `https://www.dropbox.com/s/nw63584g7hqyv92/Fabricage%20DROSs%20en%20Nb%20technologie.doc?dl=0`.

[37] Photoresist datasheet. [Online] Available from: `http://diyhpl.us/~bryan/papers2/curing/datasheets/OiR_906.pdf` [Last Accessed: Sunday 21st June, 2015].

[38] OPD developer material safety datasheet. [Online] Available from: `http://cleanroom.ien.gatech.edu/media/uploads/msds/284.pdf` [Last Accessed: Sunday 21st June, 2015].

[39] M. Podt. *Wideband low-noise integrated SQUID systems.* Phd thesis, University of Twente. Enschede, 2002, ISBN: 9036518369. **Chapter 5: Smart DROSs**. p.107.

[40] R. Monaco *et al.* **Fabrication and properties of multiple stacked Josephson tunnel junctions**.*IEEE Transactions on applied superconductivity.* **6**, April 1996.

[41] R. Kossowsky *et al. Physics and materials science of vortex states.* Kluwer Academic Publishers, 1999, ISBN:0-7923-5663-2.

[42] V. N. Gubankov *et al.* **Influence of trapped Abrikosov vortices on the critical current of the Josephson tunnel junction** . *Supercond. Sci. Technol.*. **5**, 168, 1992.

[43] A.A.Golubov *et al.* **Effect of solitary Abrikosov vortices on the properties of Josephson tunnel junctions**.*Sov. Phys. JETP.* **65**, 849, 1987.

[44] Prof. Dr. Ir. A. Brinkman, Joris Voerman (MSc). University of Twente. *Basic architecture and fabrication of a TI device.* **Conversation**, May 2015.

[45] Chuan Li (PhD). University of Twente. *Transportation of TI flakes and SQUID devices at desired locations.* **Private communication**, May 2015.

[46] C. Vieu *et al.* **Electron beam lithography: resolution limits and applications**.*Applied Surface Science.* **164**, 111-117, 200.

Citations from appendices text

[1] Xiao-Liang Qi *et al.* **Inducing a magnetic monopole with topological surface state**. *Science*, 27 February 2009, **323** (5918): 1184-1187.

[2] Prof. Dr. Ir. A. Brinkman. Chair Quantum Transport in Matter research group. University of Twente. *Discussion on initial SQUID design calculations.* **Conversation**, 16 February 2015.

[3] Clarke *et al* (ed). *The SQUID handbook.* Vol. 1: Fundamentals and technology of SQUIDs and SQUID systems. Wiley-VCH, 2004, ISBN: 3-527-40229-2. p.123.

[4] C. Brons. **Low-Tc fabrication process**. [Unpublished], April 1998, University of Twente. Available from: `https://www.dropbox.com/s/nw63584g7hqyv92/Fabricage%20DROSs%20en%20Nb%20technologie.doc?dl=0`.

[5] C. J. M. Verwijs. *Fractional flux quanta in high-Tc/low-Tc superconducting structures.* Phd thesis, University of Twente. Enschede, 2009, ISBN: 978-90-9024316-0. **Chapter 2: Superconducting loops containing Josephson junctions**.

[6] M. Cyrot *et al. Introduction to superconductivity and high-Tc materials.* World Scientific Publishing, 1992, ISBN: 9810201435. **Chapter 6: Josephson effects**.